Max-Planck-Institut für Meteorologie

REPORT No. 234

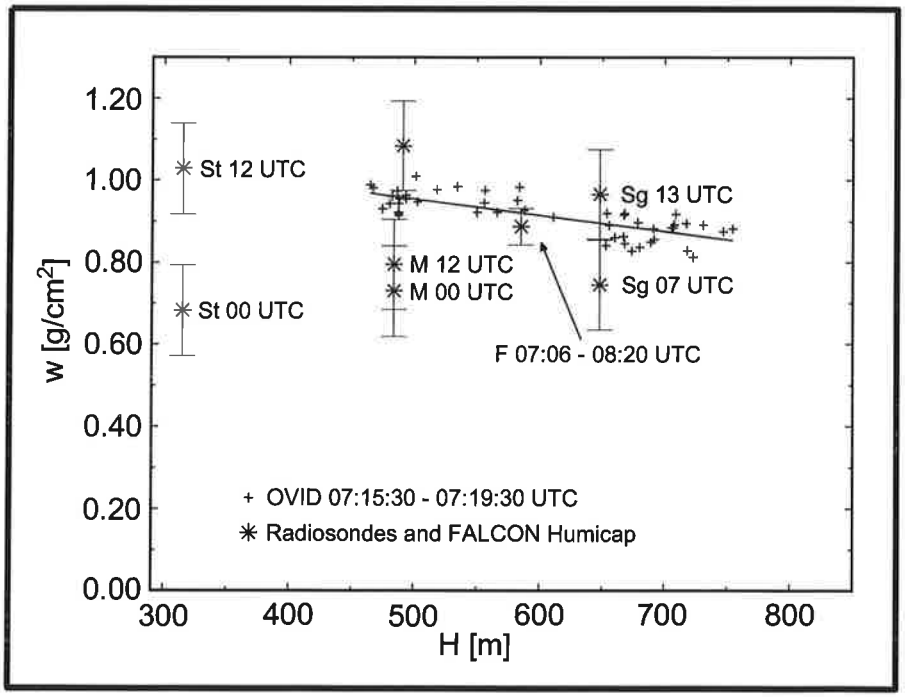

PASSIVE REMOTE SENSING OF COLUMNAR WATER VAPOUR CONTENT ABOVE LAND SURFACES

PART I: THEORETICAL ALGORITHM DEVELOPMENT
PART II: COMPARISON OF OVID MEASUREMENTS WITH RADIOSONDE AND DIAL MEASUREMENTS

by

Barbara Bartsch · Stephan Bakan · Gerhard Ehret
Jürgen Fischer · Martina Kästner · Christoph Kiemle

HAMBURG, March 1997

AUTHORS:

Barbara Bartsch	Meteorologisches Institut Universität Hamburg Bundesstr. 55 D-20146 Hamburg Germany
Stephan Bakan	Max-Planck-Institut für Meteorologie
Gerhard Ehret Martina Kästner Christoph Kiemle	Institut für Physik der Atmosphäre DLR Oberpfaffenhofen Postfach 11 16 82230 Weßling Germany
Jürgen Fischer	Institut für Weltraumwissenschaften Freie Universität Berlin Fabeckstraße 69 14195 Berlin Germany

MAX-PLANCK-INSTITUT
FÜR METEOROLOGIE
BUNDESSTRASSE 55
D - 20146 HAMBURG
GERMANY

Tel.: +49-(0)40-4 11 73-0
Telefax: +49-(0)40-4 11 73-298
E-Mail: <name> @ dkrz.de

Passive Remote Sensing of Columnar Water Vapour Content above Land Surfaces

Part I: Theoretical Algorithm Development

Barbara Bartsch, Meteorologisches Institut, Universität Hamburg, Germany

Jürgen Fischer, Institut für Weltraumwissenschaften, Freie Universität Berlin, Germany

ISSN 0937-1060

Corresponding author: Prof. Dr. Jürgen Fischer, Institut für Weltraumwissenschaften,
Freie Universität Berlin, Fabeckstrasse 69, D-14195 Berlin, Germany

Abstract

A method is presented to retrieve the total atmospheric water vapour content above land surfaces with the aid of airborne or satellite spectral measurements of backscattered solar radiation.

During algorithm development, special emphasis is given to proper description of the global variety of temperature, pressure, and water vapour profiles, as well as optical parameters of aerosols and spectral surface reflectivity values.

Sensitivity studies show that the variability of spectral surface reflectivity has the greatest impact on the errors of the derived water vapour contents. The number and location of necessary channels is therefore optimized with respect to the influence of surface reflectance. Finally the water vapour algorithm for the spectrometer MERIS on board ESA's environmental satellite ENVISAT is defined.

1. Introduction

Atmospheric water vapour is very important for many reasons. Firstly, it is the most significant greenhouse gas of the atmosphere. It influences weather and climate, and is responsible for clouds and precipitation which modulate atmospheric radiative energy transfer (Ramanathan et al. 1989). Therefore it influences the energy balance of the earth and thus also temperature and circulation of the earth-atmosphere system (Starr and Melfi 1991). The amount of water vapour determines directly the distribution and structure of clouds and therefore the precipitation pattern. That is why the knowledge of atmospheric water vapour content is of special interest e.g. for numerical weather models.

Secondly, water vapour strongly influences remotely sensed data of the earth surface. E.g. the presence of haze reduces the vegetation indices of foliated forest, derived from radiances observed by polar orbiting weather satellites (NOAA/AVHRR), to prefoliated values (Schmid et al. 1991).

Water vapour varies strongly in time and space leading to the necessity for global monitoring of atmospheric water vapour contents. AVIRIS aircraft measurements show patchy water vapour fields especially above land surfaces which can not be resolved by the use of in-situ measurements such as radiosonde data (Gao et al. 1993).

Today global detection of the total water vapour is carried out by the passive microwave sensor SSM/I (Special Sensor Microwave Imager) on-board the DMSP-satellites with a mean error in column content of 7% (Schlüssel and Emery 1990). The spatial resolution of these measurements is 49 km x 63 km, which is not sufficient to resolve mesoscale water vapour structures. The presence of non-precipitating clouds does not limit the retrieval.Marked variability in emissivity from land surfaces in the microwave region means that this method is restricted to oceanic surfaces.

With HIRS-2 (High Resolution Infrared Sounder), part of TOVS (Tiros-N Operational Vertical Sounder), a polar orbiting infrared-microwave sensor on board the NOAA satellites, total water vapour content above land surfaces is determined using 5 spectral channels between 6 and 14 μm with a relative error of 20% (Susskind et al. 1984; Starr and Melfi 1991). Problems are caused by the need to guess the temperature and water vapour profile together with surface temperature

(Gao 1993). Again the spatial resolution is not sufficient to resolve mesoscale water vapour structures. Additionally it is restricted to cloudless situations.

Besides HIRS-2 the VISSR (**V**isible-**I**nfrared **S**pin **S**can **R**adiometer) atmospheric sounder VAS (**V**ISSR **A**tmospheric **S**ounder) on board of the geostationary GOES (**G**eostationary **O**perational **E**nvironmental **S**atellite) satellites also measures the water vapour content (Starr and Melfi 1991) in the Infrared spectral range. The Infrared measurements by METEOSAT represent water vapour contents in the middle atmosphere. However, problems arise which are analogous to those encountered with HIRS-2 measurements (Hayden 1988). The estimation of errors is problematic, because the strong spatial variability of water vapour makes it difficult to compare radiosonde with moderate resolution data (Starr and Melfi 1991). Chesters (1983) indicates an accuracy of only 1 g/cm^2 in the water vapour range between 1.7 and 5.5 g/cm^2 by comparing radiosonde data with GOES/VAS measurements.

Because the present satellite water vapour remote sensing capabilities show only limited accuracy over land, various attempts are being made to develop new water vapour algorithms using other spectral regions than the thermal infrared or the microwave region.

Today spectrometers are available which fulfil the necessary specifications for measurements in the near Infrared (NIR) spectral region. Present aircraft and future satellite measurements of columnar water vapour contents already use measurements of solar radiation in the $\rho\sigma\tau$-water vapour absorption band such as proposed by various authors:

Fischer (1989) proposed a differential absorption method using two spectral bands close to each other to minimize the influence of spectrally varying surface reflectance. Based on radiative transfer simulations he estimated an accuracy of around 10% for the retrieval of the total water vapour content.

Frouin et al. (1990) also use a differential method with two spectral channels, one narrow, the other wide, both centered around 935 nm. Calculation of the total water vapour column contents by measuring downward radiance in comparison with radiosonde data shows a 15% relative error. These measurements were ground-based, where the influence of surface reflectivity can be neglected. Aircraft measurements of up-welling solar radiance during two flights yielded errors

between 13 and 18%, respectively. Unfortunately, during the theoretical algorithm development no spectral nonlinearities of surface reflectance or of atmospheric scattering parameters were taken into account. However, nonlinearities of the surface reflectivity are published by Bowker et al. (1985) for various surfaces. A further problem is the saturation effect of the narrow band channel because of the strong water vapour absorption at $\lambda = 935$ nm.

As far as satellite measurements are concerned there are three satellite projects which take advantage of the new spectrometer/imager generation in the NIR spectral range: POLDER on board ADEOS (Bouffiès et al. 1996), MODIS on board EOS (King et al. 1992), and MERIS on board ENVISAT (Morel et al. 1995).

The French POLDER (**POL**arization and **D**irectionality of the **E**arth **R**eflectances) on board the Japanese satellite ADEOS (**AD**vanced **E**arth **O**bserving **S**atellite), which will be launched in August 1996, will provide total water vapour estimates computed from two spectral channels (865 and 910 nm, 40 and 20 nm spectral halfwidth, respectively) with an expected error in the order of 10% (Bouffiès et al. 1996). However, this will lose the advantage of the same center bandwidth in the „Frouin et al. (1990)" algorithm for variations of optical parameters between the two channels.

Gao et al. (1993) are proposing at least three spectral channels for airborne/satellite water vapour remote sensing: one broadband channel around 940 nm and two narrow band channels in the window regions on both sides of the $\rho\sigma\tau$-absorption band. Under the assumption of spectrally linear variation in the optical parameters of atmospheric scattering and surface reflectivity, variations of these parameters within the $\rho\sigma\tau$-band can be estimated with the aid of the two window channels. The estimated relative error of retrieved water vapour based on theoretical calculations is around 5% for surface visibilities above 20 km. The error due to spectral nonlinear variations of surface reflectivity is estimated to be less than 8.4%. However, these investigations include only a part of the surface types used in this paper. Also no statement of the assumed water vapour content is given. On the other hand, the relative error increases with decreasing water vapour amount, as is shown in this paper.

On the basis of Gao et al. (1993) an algorithm for the NASA spectrometer MODIS on board the EOS (**E**arth **O**bserving **S**ystem) platform, which will be launched in 1998, is defined to estimate

the water vapour from measurements of five spectral channels at 865, 905, 936, 940, and 1024 nm for various conditions.

The investigation is focused on the definition of the channel location of the MERIS (**ME**dium **R**esolution **I**maging **S**pectrometer) instrument on board ESA's satellite ENVISAT which will be launched in 1999. This study concentrates on the retrieval of total water vapour over land because this is the most demanding application. For the estimation of water vapour above ocean surfaces the algorithm has to include a correction factor to take into account the aerosol optical depth which is necessary due to the low reflectivity values of water.

Various radiative transfer simulations were carried out within the spectral range 683.0 and 1034.6 nm for development of the algorithm. The radiative transfer model used in this case is validated by comparison to measured radiances. The first application of the algorithm applied to airborne spectra measured by OVID is shown in Bartsch et al. (1996).

2. Theoretical Simulations

A radiative transfer model based on the Matrix Operator method is used for development of the algorithm and validated by measurements with OVID (**O**ptical **V**isible and near **I**nfrared **D**etector), a high-resolution airborne spectrometer. The model offers the possibility of: a) combination of layers of any given optical properties, b) very fast calculation even in the case of optically thick layers with highly anisotropic phase functions, c) choice of any desired surface reflectivity, and e) the calculation of up- and down-welling radiances within the atmosphere at all layer boundaries (Plass et al. 1973).

The radiative transfer code used in this study is based on Graßl (1978) and Fischer (1983). Although azimuth resolution has been achieved, only simulations for a nadir-type geometry – adapted to the OVID measurements – are carried out here. Expansion of the algorithm to other geometries is underway.

For the development of a new water vapour algorithm, altogether 1680 spectra were calculated, including worldwide variations of the atmospheric temperature and pressure profile, aerosol optical depth, surface reflectivity and total water vapour content over land surfaces. Considered sun

zenith angles are 0.0, 19.1, 35.0, 50.7, and 66.5°. The vertical structure of the atmosphere was described by 20 homogeneous model layers. The wavelength range between 683.0 and 1034.6 nm was resolved in steps of 0.6 nm, with a spectral resolution of 1.7 nm according to the measurements of OVID. The simulations therefore cover three water vapour bands (α, μ, and $\rho\sigma\tau$) of different strength, which can be seen in Fig. 1 in detail.

The input parameters of the simulations are described in the following sections.

a. Vertical Temperature, Pressure, and Water Vapour Profiles

Vertical profiles of temperature, pressure, and water vapour are taken from worldwide radiosonde data to cover a wide range of natural variations and to avoid the smoothed profiles of the standard atmospheres (McClatchey 1972). Since the averaging of these profiles would also yield very smooth profiles, 12 profiles were chosen empirically as representing totally different surface pressure, temperature and water vapour profiles. They cover a worldwide range of atmospheric profiles. Fig. 2 shows these profiles with total water vapour column contents reaching from 0.33 to 5.57 g/cm^2. Surface temperature varies from -11.5 to 33.2°C and surface pressure from 986.9 to 1024.3 hPa. Besides a few near-surface temperature inversions, one profile shows a very strong inversion at 850 hPa.

The absorption properties of water vapour vary with pressure and temperature so that a correction factor has to be applied to the proposed water vapour algorithm for surface elevations other than mean sea level (see section 6c).

b. Aerosol Optical Parameters

The used aerosol models are described in the „Global Aerosol Data Set" GADS (Koepke et al. 1995). GADS represents a global set of aerosol optical parameters suitable for global climate simulations. Eleven aerosol components were considered within GADS: water soluble, water insoluble, soot, 3 different sea salts, 4 types of mineral aerosols, and droplets of sulfuric acid. The optical parameters of these components are determined by measurements and Mie calculations. Within GADS extinction, scattering, and absorption coefficients, single scattering albedo, and phase functions in dependence of wavelength are given. The aerosol optical parameters of the water soluble components, sea salts, and sulfuric acid droplets are dependent on the relative

humidity of the surrounding atmosphere.

The optical parameters are given for 8 humidity classes: 0, 50, 70, 80, 90, 95, 98, and 99%, where the parameter changes are most pronounced at high relative humidities. The humidity dependence of the aerosol parameters is considered within each atmospheric layer of the Matrix Operator model. Therefore the optical parameters of the aerosol vary with wavelength and atmospheric layer corresponding to the relative humidity profile of the considered atmosphere.

As far as particle number density profiles are concerned, GADS defines 10 different aerosol types consisting of different mixing ratios of the 11 different aerosol components. The aerosol optical depth is therefore given by the integration of the humidity dependent aerosol extinction properties of the considered atmosphere.

The simulations consider four of these types: „average continental", „clean continental", „urban" and „maritime polluted". The particle number densities of these chosen types are constant between ground and 1.4 or 2.2 km respectively, followed by exponential reduction up to 13 km. A constant sulfuric acid droplet profile is assumed in the stratosphere.

The strongest humidity dependence occurs for the „clean continental" type, where the optical depth varies by a factor of 8 when the relative humidity changes from 50% to 99%.

In addition to the variation of the optical depth with relative humidity and the respective aerosol type, the total aerosol extinction was varied according to a Gaussian distribution with a standard deviation of 30% around the given optical depth. The average optical depth of the aerosol at 550 nm therefore amounts to 0.21 with a standard deviation of 0.14 (minimum value: 0.03, maximum value 1.00) within the used simulations. The mean value when accounting for the slant path from the sun to the surface and vertical path back to the sensor is 0.52 with a standard deviation of 0.38 (minimum value: 0.06, maximum value: 3.5).

c. Spectral Surface Reflectivity

Together with gaseous absorption, surface reflectance is the most important factor modifying upward directed spectral solar radiances. Both the absolute value and the spectral behaviour of the surface reflectance influence water vapour retrieval.

In the literature, high resolution bidirectional spectra of surface reflectivity are rare and not suited to worldwide simulations of backscattered radiances. The present simulations consider reflectance measurements with moderate spectral resolution ($\Delta\lambda$ = 10 nm) of 22 different targets assuming Lambertian surface reflectivities, whereby the reflectance varies between 10 and nearly 100% (Bowker et al. 1985; Krinov 1953).

The assumption of Lambertian surface reflectivity does not affect the derived water vapour algorithm for two reasons. Firstly – as will be shown later in this paper – the developed water vapour algorithm makes use of neither the absolute nor the relative value of surface reflectivity. Therefore, the assumption of Lambertian reflectance within the simulations has no impact on the water vapour retrieval as long as the variety of spectral surface reflectivity values is met by the simulations, which is the second point of interest. The variety of surface reflectivity values received from the simulations coincide closely with the reflectance values seen by airborne measurements (Bartsch et al. 1997).

Different types of vegetation, snow and soil are considered in accordance with the global land surface abundance of around 53%, 13%, and 34%.

The surface reflectances depend on wavelength in a nonlinear way due to changes from chlorophyll absorption to plant cellular reflectance („red edge"), refractive index discontinuities of plant cellular constituents, absorption by iron rich soils, and absorption by solid water or ice constituents (Bowker et al. 1985; Gao et al. 1993).

Fig. 3 shows spectral surface reflectivities used in the simulations normalized to the „window-channel" reflectivity of the $\rho\sigma\tau$-absorption band at λ = 875 nm. There are distinct spectral variations for most of the considered targets. The absolute value of these nonlinearities is confirmed by airborne measurements shown in Bartsch et al. (1996).

3. Validation of the Model

There are three water absorption bands within the spectral region between 683 and 1035 nm, which are principally suitable for water vapour detection. These bands are displayed in Fig. 1 (solid line), which shows an example of backscattered radiances above a fir forest between 650 and 1000 nm. The spectra were measured by the spectrometer OVID on board an aircraft during the aircraft campaign CODEX '93 in Southern Germany at 12 UTC 15 September 1993, at a flight level of 3630 m. CODEX '93 was organized in cooperation with the **D**eutsche Forschungsanstalt für **L**uft- und **R**aumfahrt (DLR). The two oxygen bands and four Fraunhofer lines (one H- and three Ca-Fraunhofer lines) are also prominent features in such a spectrum. Conformity of the radiative transfer calculations with these measurements is also demonstrated in the Fig. 1.

Comparison of measured and simulated backscattered radiances requires definition of, various input parameters for the radiative transfer model, such as:

- spectral surface reflectance
- optical parameters of the aerosols
- water vapour profile
- temperature and pressure profile

where the latter are taken from a radiosonde measurement 30 km away at the same time because of the lack of meteorological instrumentation on board the aircraft.

The spectral step-width for the simulations – adapted to the OVID measurements – was 0.6 nm with a spectral resolution of 1.7 nm in the absorption bands, while the step-width was increased in the atmospheric window regions. The measured detector function of OVID was also introduced for the gaseous transmission calculations. Altogether 20 atmospheric layers were considered with minimum geometrical depth at the surface (200 m).

a. Spectral Surface Reflectivity

During CODEX '93 no simultaneous spectral surface reflectance measurements were carried out. Therefore, literature data had to be taken for the simulations.

However, the window radiance at 882 nm of the measured spectra varied with a standard deviation of 30.4% even over a very homogeneous fir forest within a flight distance of 3 km. This is caused by OVID's very small field of vision of just a few meters. Reflectivity values of vegetation also depend strongly on season, growth status, and environmental conditions. There are therefore problems in applying literature data of surface reflectance values to OVID measurements. However, the fir forest winter reflectance data of Krinov (1953) were taken for comparison with measurements, and had to be extrapolated for wavelengths beyond 880 nm.

b. Aerosol Optical Properties

The input aerosol parameters are chosen in correspondence to the aerosol model „average continental" of the GADS (**G**lobal **A**erosol **D**ata **S**et) which consists of water soluble and water insoluble components as well as some soot (Koepke et al. 1995). As far as surface elevations equal to mean sea level are concerned, the profile is kept constant up to 2200 m. This height was reduced to 2000 m for the surface elevation of 623 m of the measurement area according to Shettle (1989). Thereafter it undergoes exponential decrease.

The presence of cumulus clouds in the measurement area means that the optical parameters of the aerosols are chosen according to a relative humidity of 90% below 2000 m, yielding to an optical depth of 0.22.

Fig. 1 shows the comparison of the simulated (dotted line) and the measured (solid line) spectrum. The window intensities are simulated very well except in the wavelength region lower than 770 nm. This is where the so called „red edge" of vegetation is located, varying strongly even for one vegetation type in dependence on vegetation age, water abundance, and other parameters (see Bowker et al. 1985). These discrepancies are of minor importance for comparison of the simulated and the measured radiances at wavelength higher than 770 nm.

The dominant Fraunhofer lines between 850 nm and 870 nm are not taken into account within the simulations.

c. Gaseous Absorption

Simulated transmission for the oxygen absorption band at 760 nm is found to be 0.327 instead of measured 0.291. Such deviations of measured and simulated spectra when using the HITRAN data base of the O_2-A band are also found by Pflug (1993). Part of it might be due to the missing Fraunhofer lines in the simulations. The use of the Voigt absorption line shape instead of the used Lorenz line shape does not reduce this discrepancy because most of the O_2 is located within the lower atmosphere.

On the other hand the O_2-A absorption line intensities are increased by about 15% in the newest HITRAN '96 data base edition (Rothman et al. 1996) in comparison to the edition used (Rothman et al. 1992). The magnitude of the changes is consistent with the observed discrepancies with respect to oxygen absorption.

As far as the water vapour absorption bands around 820 nm and between 895 and 990 nm are concerned, there is excellent coincidence in the spectral behaviour of simulated and measured radiances. Unfortunately, no simultaneous measurements of the actual water vapour amount were available. The simulations were based on 1.81 g/cm^2 total water vapour content, corresponding to a humid atmosphere within the lower 2000 m (relative humidity of 90%). Nevertheless, the simulated absorption strength seems to be too small.

For comparison the total water vapour content derived from radiosondes launched at around 0, 12, and 24 UTC (OVID measurement time: 12 UTC) is given in Table 1 for Munich (30 km distance) and Stuttgart (210 km distance) (Deutscher Wetterdienst 1993a and b). Since the surface elevation of the measurement area is 623 m above mean sea level (msl), the water vapour content above 623 m msl is also given. However, the total water vapour above a surface elevation of 623 m msl is expected to be higher than the total water vapour above 623 m msl in the free atmosphere. That means cutting the radiosoundings below 623 m will rather underestimate the total water vapour amount within the measurement area.

As far as the absolute value is concerned, the total water vapour content used within the simulations seems to be above the values estimated from the radiosoundings. Missing water vapour values at the field location and horizontal gradients prevent an exact error estimate.

This discrepancy may also arise from the error bars of the absorption line parameters used within the model. This presumption is strengthened by the chances of the database used between the last two editions. The calculated transmission within the ρστ-absorption band varied by up to 20% for the HITRAN data base from 1992 (Rothman et al. 1992) in comparison to the HITRAN data base from 1986 (Rothman et al. 1986), when applied to the mid-latitude summer atmosphere. Furthermore, transmission discrepancies in the order of 0.1 g/cm^2 water vapour absorption can be explained by using different solar spectral irradiance data sets.

In conclusion, the spectral behaviour of the simulations and the measurements coincide closely above 770 nm where the red edge no longer influences reflectivity. Oxygen absorption will be described well when using the next HITRAN data base edition. As far as water vapour absorption is concerned, there is excellent coincidence in the spectral behaviour between measurement and simulation. However, the absorption strength is too small within the model. This conclusion is underlined by a first application of the developed algorithm to measured spectra (Bartsch et al. 1997).

But as long as there are no other more accurate spectral high-resolved water vapour absorption parameters, the use of the HITRAN database is the only chance to carry out useful radiative transfer simulations. But even in the case of line data leading to insufficient absorption, it can be assumed that only the coefficients of the proposed water vapour algorithm have to be adjusted, because the spectral behaviour is described well within the absorption bands.

Various simulations were therefore carried out to select appropriate channel locations and to define a water vapour algorithm. However, in the height of these experiences it is advisable to adapt the algorithm coefficients derived from radiative transfer calculations to spectral measurements.

4. Optimization of Channel Locations

Error analysis of the simulated spectra with respect to water vapour retrieval showed that the spectral variety of the surface reflectivity has the greatest impact on the derived water vapour error above land surfaces. The channel location is therefore optimized with respect to the disturbing surface influence in the following.

The simplest way to determine the atmospheric water vapour content w is to determine the water vapour transmission $T(w, \lambda_i)$ which is given in the monochromatic case without scattering processes as

$$T(w,\lambda_i) = \frac{L(w,\lambda_i)}{L(w=0,\lambda_i)} = e^{-c(\lambda_i)\,w} \tag{1}$$

and therefore

$$w = -\frac{1}{c(\lambda_i)} \cdot \ln\left(\frac{L(w,\lambda_i)}{L(w=0,\lambda_i)}\right) \tag{2}$$

with $L(w, \lambda_i)$ measured solar radiance at the absorption wavelength λ_i after passing the water vapour content w, and $c(\lambda_i)$ absorption coefficient at wavelength λ_i. Pressure and temperature are assumed to be constant.

In contrast to $L(w, \lambda_i)$, which is measured, $L(w = 0, \lambda_i)$ has to be estimated on the basis of a wavelength λ_a with no or only small water vapour absorption, referred to below as the „window channel". This window channel λ_a must be selected very close to the absorption wavelength λ_i in order to reduce spectral variations of atmospheric and surface optical properties between the two channels. The window channels corresponding to the three absorption bands used during this investigation are marked in Fig. 4, showing the transmission of the mid-latitude summer atmosphere of McClatchey et al. (1972).

With $\Delta L(w =0, \lambda_i)$ the error of the estimation of $L(w = 0, \lambda_i)$, the relative error of the derived water vapour content is given according to error propagation rules as:

$$\frac{\Delta w}{w} = -\frac{\Delta L(w=0,\lambda_i)}{L(w=0,\lambda_i)} \cdot \frac{1}{\ln\dfrac{L(w,\lambda_i)}{L(w=0,\lambda_i)}} = -\frac{\Delta L(w=0,\lambda_i)}{L(w=0,\lambda_i)} \cdot \frac{1}{\ln\left(T(w,\lambda_i)\right)} \tag{3}$$

The spectral surface reflectivity has the greatest impact on spectral variations of $L(w = 0, \lambda_i)$ above land surfaces and clear atmospheres. The consequent neglection of atmospheric scattering

and aerosol absorption processes yields to

$$\frac{\Delta L\,(w=0,\lambda_i)}{L\,(w=0,\lambda_i)} \approx \frac{\Delta R\,(\lambda_i)}{R\,(\lambda_i)} \tag{4}$$

with $R(\lambda)$ the spectral surface reflectivity.

Therefore, the relative error of the retrieved water vapour content is given as

$$\frac{\Delta w}{w} \approx -\frac{\Delta R\,(\lambda_i)}{R\,(\lambda_i)} \cdot \frac{1}{\ln\left(\dfrac{L\,(w,\lambda_i)}{L\,(w=0,\lambda_i)}\right)} = -\frac{\Delta R\,(\lambda_i)}{R\,(\lambda_i)} \cdot \frac{1}{\ln\,(T\,(w,\lambda_i))} \tag{5}$$

The surface reflectivity values published by Bowker (1985) were used for the following investigations of $\Delta w/w$ for various land surfaces. The study concentrated on these 112 reflectivity spectra which belong to the surfaces types vegetation, snow, or soil and which cover the wavelength region between 680 and 1050 nm. The global abundance of vegetation, soil, and snow was stated according to climate models (53% vegetation, 34% soil, and 13% snow). However, for the interpretation of the results it has to be assumed that the published surfaces are representative of the global average.

The study was carried out for the „mid-latitude summer atmosphere" with a total water vapour content of 2.9 g/cm^2 (McClatchey et al. 1972). The three water vapour absorption bands between 650 and 1050 nm were taken into account. Three separate investigations for each absorption band were conducted with either one window channel to the left or right of the corresponding absorption band, or with two window channels, one at each side of the considered absorption band. The location of the absorption channel was varied continuously throughout the absorption band in question.

a. Use of Two Spectral Channels

When only two spectral channels are available for water vapour remote sensing, such as proposed for MERIS (Morel at al. 1995), the window channel λ_a is chosen to the left or right of the investigated absorption band as shown in Fig. 4. The absorption channel λ_i is located within the absorp-

tion band.

In this case $R(\lambda_i)$ has to be estimated from $R(\lambda_a)$:

On the basis of the 112 surfaces the mean global surface reflectivity ratio $\overline{m}(\lambda_i, \lambda_a)_{glob}$ is determined for every wavelength pair (λ_a, λ_i).

For surface number j the reflectivity ratio $m(\lambda_i, \lambda_a, j)$ is defined as:

$$m(\lambda_i,\lambda_a,j) := \frac{R(\lambda_i,j)}{R(\lambda_a,j)} \tag{6}$$

After classification of the land surfaces j according to vegetation, soil and snow, the mean global surface reflectivity ratio can be expressed as:

$$\overline{m}(\lambda_i,\lambda_a)_{glob} = 0.53 \cdot \frac{1}{v} \sum_{j=1}^{v} m(\lambda_i,\lambda_a,j) + 0.34 \cdot \frac{1}{b} \sum_{j=v+1}^{b+v} m(\lambda_i,\lambda_a,j) + 0.13 \cdot \frac{1}{s} \sum_{j=b+v+1}^{b+v+s} m(\lambda_i,\lambda_a,j) \tag{7}$$

with v, b, and s being the number of different vegetation, soil, and snow surfaces (v + b + s = 112), respectively. The three surface types are globally distributed as 53% vegetation, 13% snow, and 34% soil. Finally the ratio $\overline{m}(\lambda_i, \lambda_a)_{glob}$ will be used for the estimation of $R(\lambda_i)$ from $R(\lambda_a)$. Therefore, it follows:

$$\Delta R(\lambda_i) = \left| \overline{m}(\lambda_a,\lambda_i)_{glob} \cdot R(\lambda_a) - R(\lambda_i) \right| \tag{8}$$

Now all parameters are known for a given atmosphere to determine the error of the derived water vapour content according to Eq. (5) with $T(w, \lambda_i)$ being the calculated transmission of the „mid-latitude summer atmosphere".

The relative error $\Delta w/w$ was calculated for all 112 surfaces, all wavelengths λ_i with stepwidth of

0.6 nm within the three absorption bands, and with λ_a right ($\lambda_a > \lambda_i$) or left ($\lambda_a < \lambda_i$) of the absorption band.

Finally the mean global error in dependence of λ_i was determined according to the global land coverage of the surface types where only those surfaces with $\Delta w/w < 50\%$ were considered. In case of a larger error it is assumed that those values will be detected as incorrect during the operational application.

Fig. 5 shows the retrieved error for the three absorption bands. The window channel λ_a is chosen at the left side of the considered absorption band (λ_a = 712, λ_a = 806, and λ_a = 890 nm, respectively). The dots represent the deviations induced by the effect of the spectral albedo of the different surfaces with respect to water vapour remote sensing; the solid line represents the global error of water vapour detection above land. The actual water vapour content was chosen as 2.92 g/cm^2. The induced relative error naturally decreases with increasing water vapour amount.

From Fig. 5 it can be concluded that the $\rho\sigma\tau$-absorption band is less influenced by spectral variations of the surface reflectivity. The global error is minimal for the channel combination λ_a = 890 nm and λ_i = 900 nm ($\Delta w/w$ = 2.5%). Results of nearly similar quality are obtained with λ_i = 935 nm ($\Delta w/w$ = 2.5%) or λ_i = 816 nm ($\Delta w/w$ = 3.5%). However, for these two absorption channels some surfaces had to be excluded in the analysis which would yield $\Delta w/w > 50\%$.

The maximum error Δw/w of the absorption channel 900 nm for a single surface is about 15%. This maximum error value was also measured during an aircraft measurement campaign above a variety of different surface types described in Bartsch et al. (1996) with nearly the same water vapour path amount. The spectral behaviour of the used surface reflectivity values seems to be representative for land surfaces, therefore.

The error increases with decreasing water vapour content. For example the mean global error is doubled for 0.73 g/cm ^{2} atmospheric water vapour content compared to 2.92 g/cm^2.

Use of the right window channel (λ_a = 745, λ_a = 847, and λ_a = 995 nm, respectively) results in 935 nm as the best choice for the absorption channel. However, the mean global error of 3.5% for the combination 890/935 nm exceeds the error by 1% when the the combination 890/900 nm is

applied. Furthermore, todays spectrometric material Silicium has only low sensitivity around 1000 nm, again recommending the window channel at 890 nm instead of at 995 nm.

Use of the α-absorption band between 700 and 740 nm results in mean global errors of more than 20% for both λ_a left or right of the absorption band, respectively. This is caused by the variability of the „red edge" (section 2c). The use of the α-absorption band is therefore not recommended for water vapour remote sensing above land.

Altogether it can be concluded that the combination 890/900 nm should be chosen for airborne/ satellite water vapour remote sensing in the solar spectral region when only two spectral channels are available. A further combination suitable for water vapour remote sensing according to this investigation is 935/995 nm.

b. Use of Three Spectral Channels

If three spectral channels are available for the remote sensing of water vapour, the two window channels $\lambda_{a,r}$ and $\lambda_{a,l}$ on the right and left side of the absorption band are possible candidates for determining $L(w = 0, \lambda_i)$. Radiance $L(w = 0, \lambda_i)$ will be calculated by using a linear interpolation between $L(\lambda_{a,r})$ and $L(\lambda_{a,l})$.

Figure 6 shows the mean global error of the retrieved water vapour content with λ_i within the absorption band and with two window channels right and left of the absorption band ($\lambda_{a,r}$ and $\lambda_{a,l}$). Again, the dots represent the error related to single surfaces. Surfaces with errors $\Delta w/w$ larger than 50% were not taken into consideration because water vapour values obtained for such surfaces are expected to be erroneous.

As expected the errors are smaller when two reference channels are used instead of only one window channel. The spectral region between 807 and 832 nm is most suitable ($1.5\% < \Delta w/w < 3.6\%$) for broadband absorption measurements (spectral halfwidth 25 nm). The absorption channels at 900 and 935 nm are also suitable ($\Delta w/w = 1.6\%$) for narrow-band measurements (spectral halfwidth ≤ 10 nm).

Only up to two surfaces with $\Delta w/w > 50\%$ had to be excluded for the spectral range 807 to 832 nm (potatoes, granite) as well as for 900 and 935 nm (biotite granite sample, limestone),

respectively. The number of excluded surfaces increases strongly for lower water vapour content.

Within the α-absorption band around 700 nm the global errors are now about 10% which is still too high for water vapour remote sensing purposes.

c. Results

A further disturbing factor in water vapour remote sensing is the atmospheric scattering due to aerosol and air molecules. These influences decrease with increasing wavelength, which again favour the ρστ-absorption band, resulting in the use of the spectral regions around 900 and 935 nm. In the case of broadband measurements the μ-absorption band around 800 nm might also be considered.

5. Eigenvector Analysis

As already described in section 2, a series of 1680 spectra was simulated to which a normally distributed noise of 1% was added. According to the findings of the previous section, the ρστ-absorption band was investigated with the aid of a principal component analysis. The first four eigenvectors explain 99.95% of the variance of all spectra (Fig. 7).

The first eigenvector represents radiances of the atmospheric window. The third is related to spectral variations of aerosol scattering and surface reflectivities. Finally, the second and the fourth are correlated with water vapour absorption. The absorption due to water vapour has to be described by two eigenvectors to account for the nonlinear effects of the absorption.

The use of the weight ratio between the first two eigenvectors as an input parameter for a one stage water vapour regression results in a rms error of 8.6% of the retrieved water vapour content. The use of a two stage regression over the weight of the first eigenvector which can also be interpreted as an indicator of the absolute surface reflectivity value, reduces the rms error to 5.1%.

Fig. 8 shows the rms error of the retrieved water vapour content versus the water vapour path w_p, which means the integrated water vapour in the slant path from the sun to the surface and back to the satellite. The relative error is largest for small water vapour contents.

Altogether it can be concluded that two spectral channels are necessary to derive the atmospheric water vapour content with an accuracy of about 5% rms error. Bearing the results of the previous sections in mind, a water vapour algorithm with respect to the MERIS instrument is developed on basis of the wavelength combination 890/900 nm. We also studied the combinations 890/935 nm, 935/990 nm, and 890/935/990 nm.

6. Water Vapour Algorithm Using the Channels 890 and 900 nm

a. Algorithm Description

The previously discussed spectra were simulated in spectral steps of 0.6 nm with a spectral resolution of 1.7 nm, adapted to the mainly used grating of OVID. 17 „OVID" channels have been averaged for the simulations of MERIS channels with a spectral resolution of 10 nm. The central wavelengths in vacuum resulted in 890.1 and 900.3 nm, respectively. For the development of a water vapour algorithm, a 3% absolute and a 0.1% relative Gaussian distributed error was also added to the simulated spectra to account for MERIS measurement errors.

Best results are achieved by applying a two stage regression approach: First the radiance ratio

$$T := L(900.3nm)/L(890.1nm) \tag{9}$$

is used where L denotes the nadir radiance.

Apparently, T is a function of the so-called integrated water vapour path w_p, which is the water vapour on the slant path from the sun to the surface and back to the sensor.

Fig. 9 shows the dependence on T for all simulations on the water vapour path w_p. The regression with

$$w_p = 224.3 - 697.0 \cdot T + 735.7 \cdot T^2 - 264.0 \cdot T^3 \quad , \quad w_p in\,[g/cm^2] \tag{10}$$

was estimated and is also plotted in Fig. 9. The rms error of the retrieved water vapour content is 7.3%.

Figure 10 shows the relative error of the water vapour content derived with Eq. (10) as a function of the logarithm window radiance L(890.1 nm) normalized to vertical incidence. A second regression is applied, therefore, which corrects different absolute reflectivity values of the surface, for which the window radiance normalized to vertical incidence is a good estimation.

The corrected water vapour path $w_{p,c}$ is now given by:

$$w_{p,c} = \frac{w_p}{0.55 + 0.10 \cdot \ln \frac{L(890.1nm)}{\cos\theta}} \tag{11}$$

With this two stage regression the rms error is reduced to 5.2%.

b. Error Analysis

The relative error of the water vapour path $w_{p,c}$ as a function of $w_{p,c}$ is shown in Fig. 11. The highest relative errors occur for low water vapour contents. The solid lines represent the error which would occur if in Eq. (10) T is varied by ± 0.015 due to reasons not attributable to water vapour variations. This error seems to be an upper limit of the expected error.

Variations of T by ± 0.015 are caused mainly by variations of the surface reflectivity ratio R(900 nm)/R(890 nm) around the global average value. This can be seen in Fig. 12 where the relative error of the retrieved water vapour is shown depending on the spectral ratio of the surface reflectivities at 900 and 890 nm for water vapour paths less than 0.8 g/cm^2. The average value of the reflectivity ratio is 0.990 and the maximum deviation is 0.018. This deviation coincides closely well with the expected variation of T by ± 0.015 because the atmosphere weakens the effect of the surface reflectivity on the radiance ratio.

Deviations in the spectral reflectivity ratio R(900 nm)/R(890 nm) from the global average cause the highest errors in received water vapour for low water vapour content. Exact knowledge of the spectral reflectivity ratio can reduce the error from about 40% to about 10%. For higher water

vapour contents the influence is less. For 20 g/cm^2 water vapour path, only 5% error are caused by an unknown reflectivity ratio.

The relative measurement error has to be less than 1.5% because this already causes uncertainties of up to 40% in the retrieved water vapour content for low water vapour amounts.

The remaining errors are due to variable atmospheric optical properties and highly variable absolute reflectivity values of the earth surface, measurement errors, and variable atmospheric profiles of temperature and water vapour. In general, these errors are small in comparison to the already studied error sources.

c. *Influence of Surface Topography*

A first error analysis with respect to surface elevation points to an underestimation of column water vapour content of ≈ 3% for 500 m topographic changes, if the algorithm is not adapted to the correct surface elevation.

For surface elevations between 350 and 850 m msl, the correction can be realized by:

$$w_{p,c,o} = \frac{w_{p,c}}{a_o + a_1 \cdot H + a_2 \cdot H^2} \qquad (12)$$

with $a_o = 0.98$, $a_1 = 3.7$ e-5, $a_2 = -9.8$ e-08 and H the surface elevation in meters. The remaining error of the retrieved water vapour content induced by variable surface elevation is about 0.5%.

7. Other Channel Combinations

a. *Use of Two Channels at 890 and 935 nm*

Although absorption at 935 nm is much stronger than that at 900 nm, the rms error of the retrieved total water vapour using the channels 890 nm/935 nm is 7.8% in comparison to 5.2% for the proposed algorithm with 890 nm/900 nm. Even for low water vapour, contents the channel combination 890 nm/900 nm predicts water vapour more precisely than the combination 890 nm/ 935 nm, which is more sensitive to absorption processes by water vapour (compare Fig. 12 with

Fig. 13).This is due to the spectral variability of the surface reflectance. The larger distance between the two wavelengths results in stronger changes in reflectivity which cannot be compensated by greater absorption of water vapour at $\lambda = 935$ nm. The mean reflectivity ratio is 0.90 with a maximum deviation of 0.22, whereas the maximum deviation for the use of channels 890 nm/ 900 nm was 0.018, which is less by one order of magnitude.

b. Use of Two Channels at 935 and 990 nm

The situation concerning the wavelength combination 935 nm/990 nm is nearly the same as for the combination 890 nm and 935 nm. The rms error is 8.6% due to the large spectral distance between the absorption and the window channel with marked variations in surface and atmospheric parameters.

c. Use of Three Channels at 890, 935, and 990 nm

More precise estimation of reflectivity changes might be achieved by using an additional third channel at the other side of the absorption band (section 4b). When the linearly interpolated radiance L_i(935 nm) is used between the window channels 890 nm and 990 nm instead of only L(890 nm) for calculating the ratio T similar to Eq. (9), the rms error is reduced to 6%. The remaining deviations are due to nonlinear spectral dependences on surface reflectivity and atmospheric extinction which cannot be estimated from the window channel radiances.

8. Summary

A number of radiative transfer simulations were carried out to develop a water vapour remote sensing technique above land using the solar spectral range. The radiative transfer model is validated by comparison with multi-spectral radiances measured by the airborne spectrometer OVID.

A 0.03 deviation in transmission was found for oxygen absorption, which is sure to be reduced by using the next HITRAN 1996 data base edition with about 15% higher absorption line intensities for the O_2-A band (Rothman et al. 1996). The magnitude of these changes is consistent with the deviation in respect of oxygen absorption.

As far as water vapour is concerned, the simulated absorption strength also seems to be too small. However, the deviations can be explained by the existing error bars of the HITRAN 1992 data base. In this case, only the coefficients of the algorithm have to be adapted for a range of simultaneously measured water vapour contents, since the spectral behaviour is simulated very well.

The simulations gave special emphasis to proper description of the global spectral surface reflectivity variability and aerosol parameters, to which a Gaussian noise of 30% was added. The aerosol properties were treated humidity-dependent. The used vertical profiles of temperature, water vapour, and pressure cover worldwide measured radiosonde data.

Sensitivity studies showed that spectral variations of the surface reflectivities between the channels used for water vapour remote sensing have the greatest impact on the derived error.

The two channels at 890 nm and 900 nm are found to be the most suitable predictors for water vapour content. This study supports the choice for the channel combination 890 nm/900 nm for the future MERIS measurements such as discussed by Fischer (1989). With a spectral resolution of 10 nm as recommended for MERIS, the rms error of the retrieved water vapour content is found to be 5.2%. A two stage regression – first for the radiance ratio L(900 nm)/L(890 nm) and then for the logarithm of the window radiance normalized to vertical incidence ln(L(890 nm)/ $\cos\theta$) – has to be applied.

The greatest relative errors occur for low water vapour contents which are caused by deviations of the spectral reflectivity ratio from the global average. Exact knowledge of the spectral reflectivity ratio can reduce the error from about 40% to about 10% for low water vapour content. For higher water vapour contents, the influence is less. For 20 g/cm^2 water vapour path, only 5% of the 10% error are dedicated to the unknown reflectivity ratio.

Since realistic measurement errors are already included in this study, it can be predicted that the spectral resolution and radiometric sensitivity of the MERIS instrument will enable us to observe water vapour fields with a spatial resolution of 1.2 by 1.2 km^2.

Other wavelength combinations, especially using 935 nm with high absorption due to water vapour, are less suitable because of the larger spectral distance from the window channel. This

results in an enhanced impact of spectral reflectivity and atmospheric scattering properties on the retrieval process.

Preparations are in progress to extend the algorithm to other viewing angles. The retrieval of total water vapour above water surfaces is less demanding. It is only restricted by the low reflectances of water surfaces. However, a summation of several pixels will enhance the signal to noise ratio which is not restricted to the spatial resolution of water fields, since there are fewer horizontal structures above oceans. The aerosol optical depth also measured by MERIS is expected to be one necessary input parameter for water vapour retrieval above water.

Due to the existing problems of simulating the absorption strength with the necessary accuracy spectral measurements are recommended to correct theoretical derived algorithm coefficients.

A first application of the developed algorithm to airborne measured OVID data is shown in Bartsch et al. (1996).

Acknowledgement

This work was supported by the German BMBF (Bundesministerium für Bildung und Forschung) project „Spektral hochauflösende Messungen rückgestreuter Strahlung über Wolken im Spektralbereich $\Delta\lambda = 0.2 - 4.5$ µm“.

REFERENCES

Bartsch, B., S. Bakan, G. Ehret, J. Fischer, M. Kästner, and C. Kiemle, 1997: Passive Remote Sensing of Columnar Water Vapour Content above Land Using the Solar Spectral Range, Part II: Comparison of OVID Measurements with Radiosonde and DIAL Measurements, submitted to *J. Appl. Met.*

Bowker, D. E., R.E. Davis, D. L. Myrick, K. Stacy, and W.T. Jones, 1985: Spectral reflectances of natural targets for use in remote sensing studies, *NASA Ref. Publ., 1139*, pp. 181.

Bouffiès, S., F. M. Bréon, D. Tanré, and P. Dubuisson, 1996: Atmospheric water vapor estimate by a differential absorption technique with the POLDER instrument, submitted to *J. of Geophysical Research.*

Chesters, D., L.W. Uccellini, W.D. Robinson, 1983: Low-Level Water Vapour Fields from the VISSR Atmospheric Sounder (VAS) 'Split Window' Channels, *Journal of Climate and Appl. Meteor.*, **22**, 725-742.

Deutscher Wetterdienst, 1993a: Europäischer Wetterbericht, Bodenwettermeldungen, Beilage 1, Jahrgang 18.

Deutscher Wetterdienst, 1993b: Europäischer Wetterbericht, *Amtsblatt des Deutschen Wetterdienstes, Aerologische Wettermeldungen, Beilage 2*, Jahrgang 18.

Fischer, J., 1983: Fernerkundung von Schwebstoffen im Ozean, *Hamburger Geophysikalische Einzelschriften*, **65**, pp. 105.

Fischer, J., 1989: Clouds Satellite Observations: High Resolution Spectroscopy for Remote Sensing of Physical Cloud Properties and Water Vapour, *Current Problems in Atmospheric Radiation*, IRS'88, Lenoble and Geleyn (Eds.), 151-154.

Frouin, R., P.-Y. Deschamps, and P. Lecomte, 1990: Determination from space of atmospheric total water vapour amounts by differential absorption near 940 nm: Theory and airborne verification, *J. Appl. Meteor.*, **29**, 448-460.

Gao, B.-C., A.F.H. Goetz, Ed R. Westwater, J.E. Conel, and R.O.Green, 1993: Possible near-IR channels for remote sensing precipitable water vapour from geostationary satellite platforms, *J. Appl. Meteor.*, **32**, 1791-1801.

Graßl, H., 1978: Strahlung in getrübten Atmosphären und in Wolken, *Hamburger Geophysikalische Einzelschriften*, **37**, pp. 136.

Hayden, C.M., 1988: GOES-VAS Simultaneous Temperature-Moisture Retrieval Algorithm, *J. Appl. Meteor.*, **27**, 705-733.

King, M.D., J.Y. Kaufmann, W.P. Menzel, and D. Tanre, 1992: Remote sensing of cloud, aerosol and water vapour properties from the Moderate Resolution Imaging Spectrometer (MODIS). IEEE Trans. Geoscience and Remote Sensing, **30**, 1, pp. 2-27.

Koepke, P., M. Hess, I. Schult, and E. Shettle, 1995: Global Aerosol Data Set, *IUGG XXI General Assembly, Abstracts Week B, B238*, Boulder, Colorado.

Krinov, E.L., 1953: Spectral reflectance properties of natural formations, *National Research Council of Canada, Technical Translation TT-439*, from Aero Methods Laboratory, Academy of Sciences, U.S.S.R., translated by G. Belkov, pp. 268.

McClatchey, R.A., R.W. Fenn, J.E.A. Selby, F.E. Volz, and J.S.Garing, 1972: Optical Properties of the Atmosphere (Third Edition), *Air Force Cambridge Research Laboratories, Environmental Research Papers*, 471, AFCRL-72-0497.

Morel, M., J.L. Bezy, F. Montagner, A. Morel, and J. Fischer, 1995: ENVISAT's Medium Resolution Imaging Spectrometer: MERIS, *ESA Bulletin 76*, pp. 40-46.

Pflug, B., 1993: Atmospheric Transmission in the O_2-A-band: Comparison of Calculations and Measurements, *Workshop Proceedings 'Atmospheric Spectroscopy Applications' - ASA Reims 93*, University of Reims Champagne Ardenne, France, September 8 - 10, 68-71.

Plass, G.N., G.W. Kattawar, and F.E. Catchings, 1973: Matrix Operator Theory of Radiative Transfer. 1: Rayleigh Scattering, *Appl. Opt.*, **12**, No. 2, 314-329.

Ramanathan, V., B.R. Barkstrom, and E.F. Harrison, 1989: Climate and the Earth's radiation budget, *Phys. Today*, **42**, 22-32.

Rothman, L.S., R.R. Gamache, A Goldman, L.R. Brown, R.A. Toth, H.M. Pickett, R.L. Poynter, J.-M. Flaud, C. Camy-Peyret, A. Barbe, N. Husson, C.P. Rinsland, M.A. Smith, 1987: The HITRAN Database: 1986 edition, *Appl. Optics*, **26**, No. 19, pp. 4058-4097.

Rothman, L.S., R.R. Gamache, R.H. Tipping, C.P. Rinsland, M.A.H. Smith, D.C. Benner, V. Malathy Devi, J.-M. Flaud, C. Camy-Peyret, A. Perrin, A. Goldman, S.T. Massie, L. R. Brown, R.A. Toth, 1992: The HITRAN Molecular Database: Editions of 1991 and 1992, *J. Quant. Spectrosc. Radiat. Transfer*, **48**, No. 5/6, 469-507.

Rothman, L.S. et al. 1996: HITRAN 1996 CDROM, available from L.S. Rothman, PL/GPOS, 29 Randolph Road, Hanscom AFB, MA01731/3010, USA.

Schlüssel, P. and W.J. Emery, 1990: Atmospheric water vapour over oceans from SSM/I Measurements, *J. Remote Sensing*, **11**, 753-766.

Schmid, B., C. Mätzler, and E. Schanda, 1991: Temporal evolution of vegetation indices and atmospheric effects, *Proceedings of the 11th EARSeL Symposium*, Graz, Austria, 3-5 July 1991, 355-368.

Shettle, E. P., 1989: Comments on the use of LOWTRAN in transmission calculations for sites with the ground elevated to sea level, *Appl. Optics*, **28**, 1451-1452.

Starr, D.O'C. and S.H. Melfi (eds.), 1991: The Role of Water Vapour in Climate, A Strategic Research Plan for the Proposed GEWEX Water Vapour Project (GVaP), *NASA Conference Publ. 3210*, pp. 60.

Susskind, S., J. Rosenfield, and D. Reuter, 1984: Remote sensing of weather and climate parameters from HIRS2/MSU on TIROS-N., *J. Geophys. Res.*, **89**, 4677-4697.

List of Figures

FIG. 10: Relative error of the water vapour retrieval using the first regression (shown in Fig. 9) depending on the logarithm of the window radiance L(890.1 nm) normalized to vertical incidence. Big crosses represent water vapour path $w_p > 2.5$ g/cm^2, small stars stand for $w_p < 2.5$ g/cm^2. The linear regression (solid line) is carried out only for the big crosses (see text below).

FIG. 11: Relative error of water vapour path after two regressions in dependence on actual water vapour path w_p.

FIG. 12: Relative error after two regressions of water vapour path less than 0.8 g/cm^2 in dependence on the surface reflectivity ratio R(900 nm)/R(890 nm).

FIG. 13: Relative error of water vapour path after the two stage regression for $w_{p,c}$ less than 0.8 g/cm^2 in dependence on the surface reflectivity ratio R(935 nm)/R(890 nm).

List of Tables

Table 1:

Time	Total Water Vapour Content at			
	Munich above		Stuttgart above	
	agl	623 m msl	agl	623 m msl
0 UTC	1.65	1.52	1.90	1.70
12 UTC	1.46	1.36	1.43	1.18
24 UTC	1.89	1.74	2.02	1.77

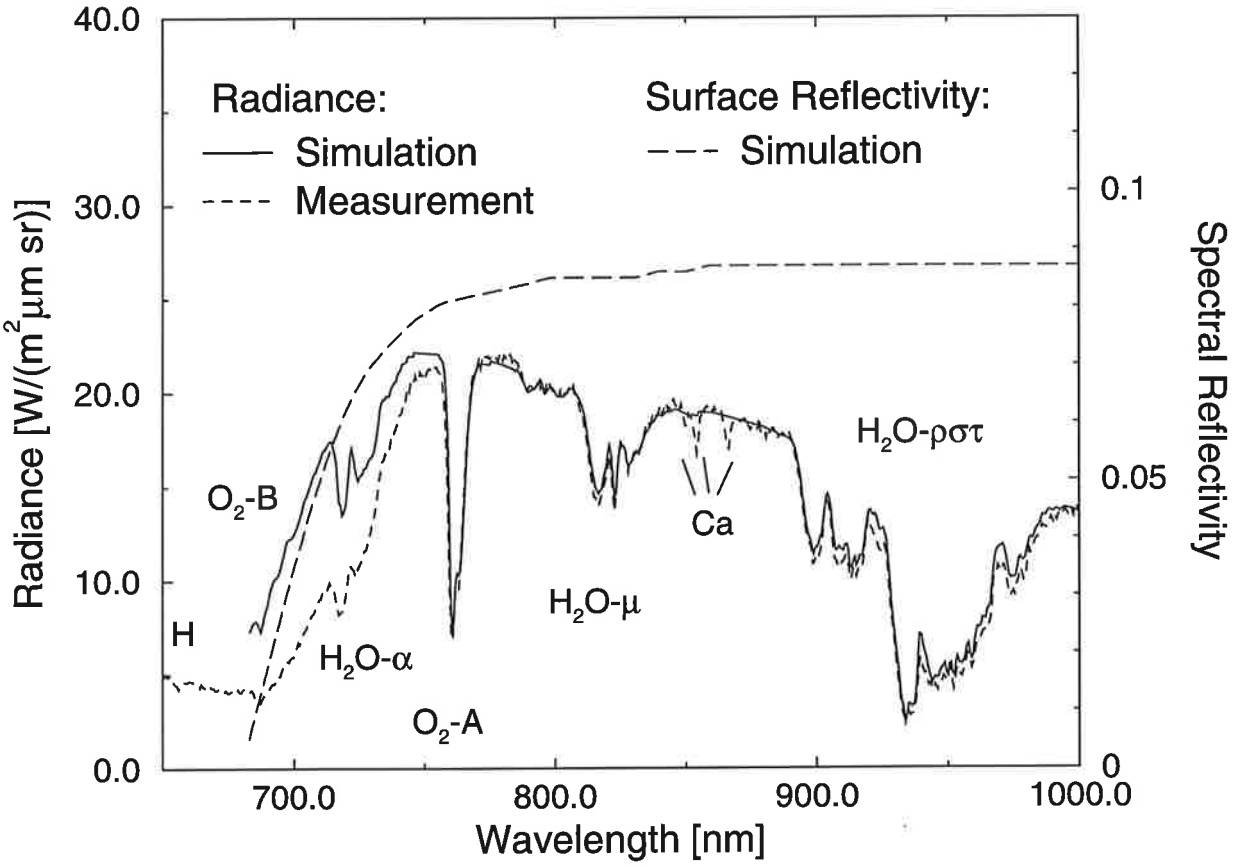
Radiance:
Simulation
Measurement
Surface Reflectivity:
Simulation
O2-B
H
H2O-α
O2-A
H2O-μ
Ca
H2O-ρστ
Radiance [W/(m2μm sr)]
Spectral Reflectivity
Wavelength [nm]
40.0
30.0
20.0
10.0
0.0
0.1
0.05
0
700.0
800.0
900.0
1000.0

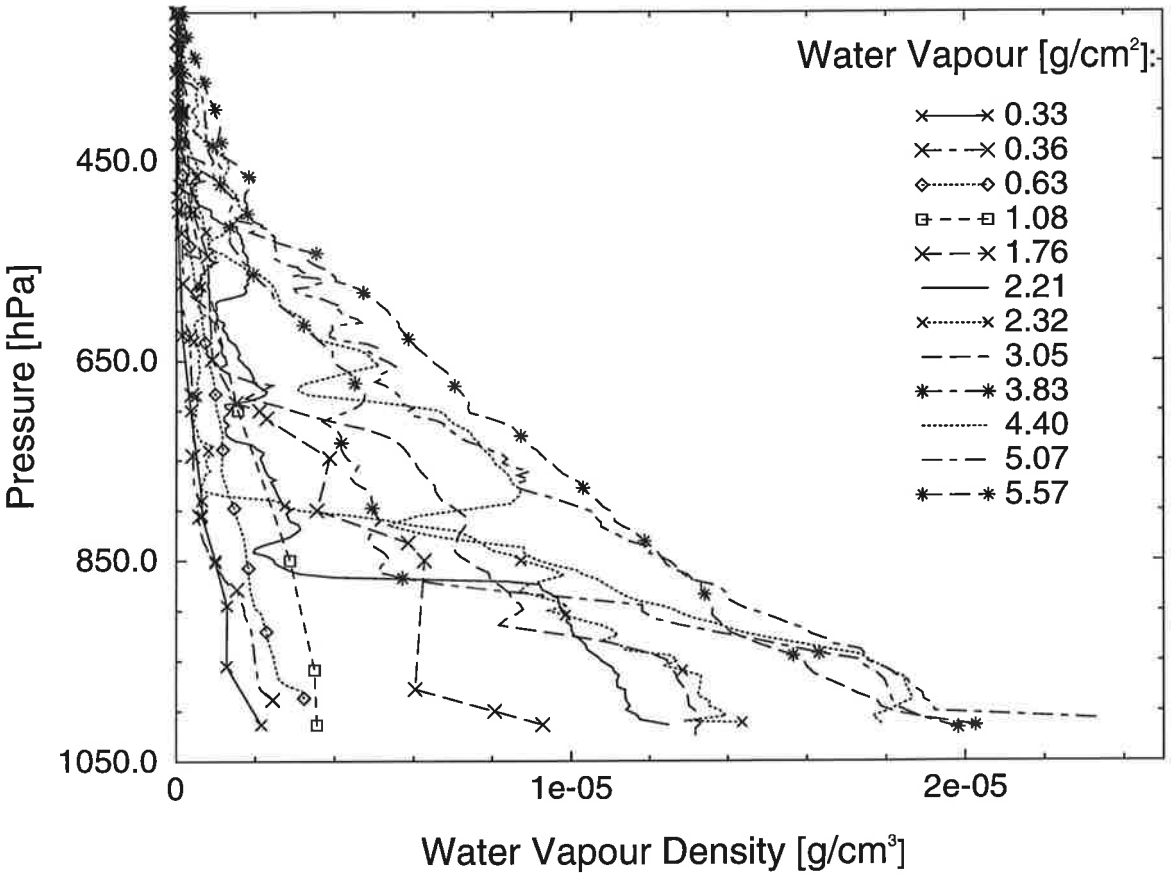
Water Vapour [g/cm²]:
0.33
0.36
0.63
1.08
1.76
2.21
2.32
3.05
3.83
4.40
5.07
5.57
Pressure [hPa]
450.0
650.0
850.0
1050.0
0
1e-05
2e-05
Water Vapour Density [g/cm³]

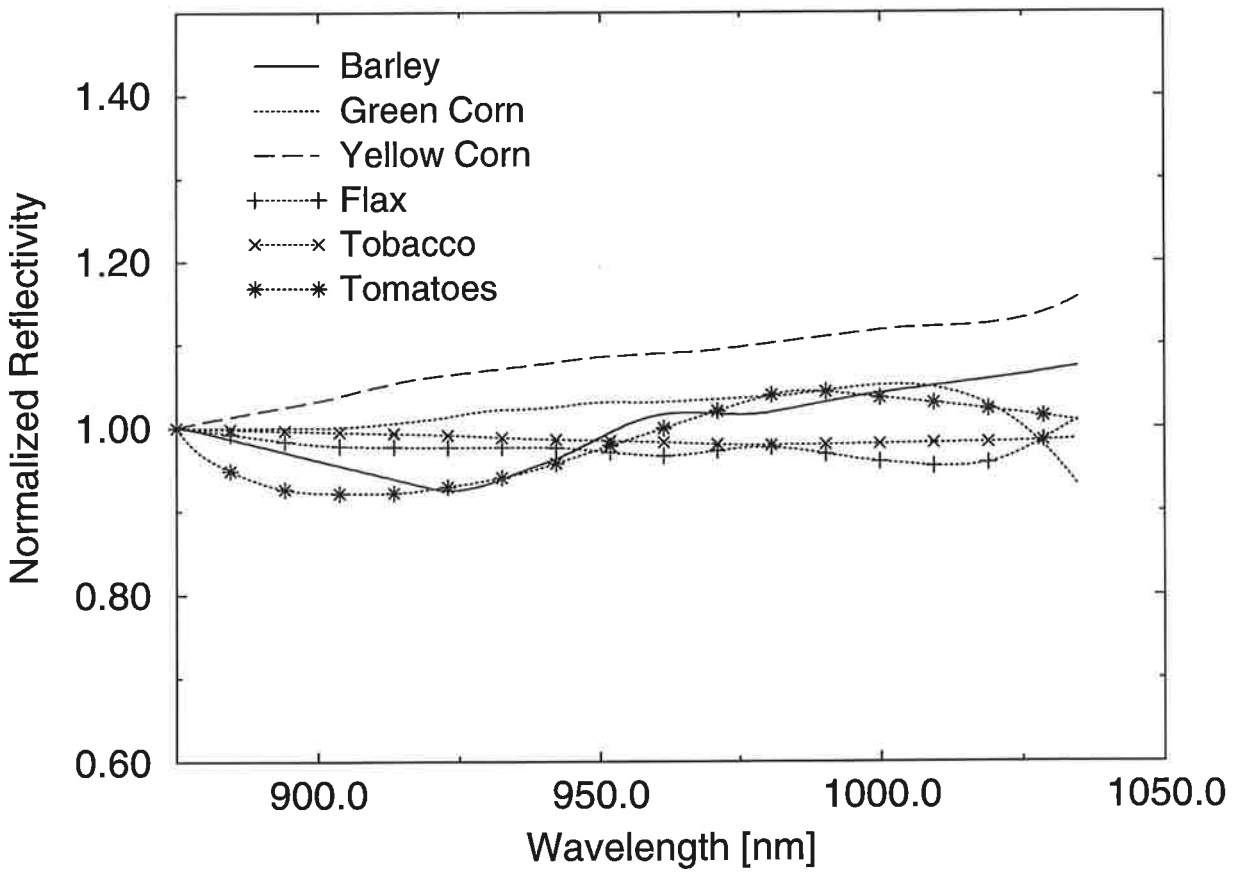
Barley
Green Corn
Yellow Corn
Flax
Tobacco
Tomatoes
Normalized Reflectivity
1.40
1.20
1.00
0.80
0.60
900.0
950.0
1000.0
1050.0
Wavelength [nm]

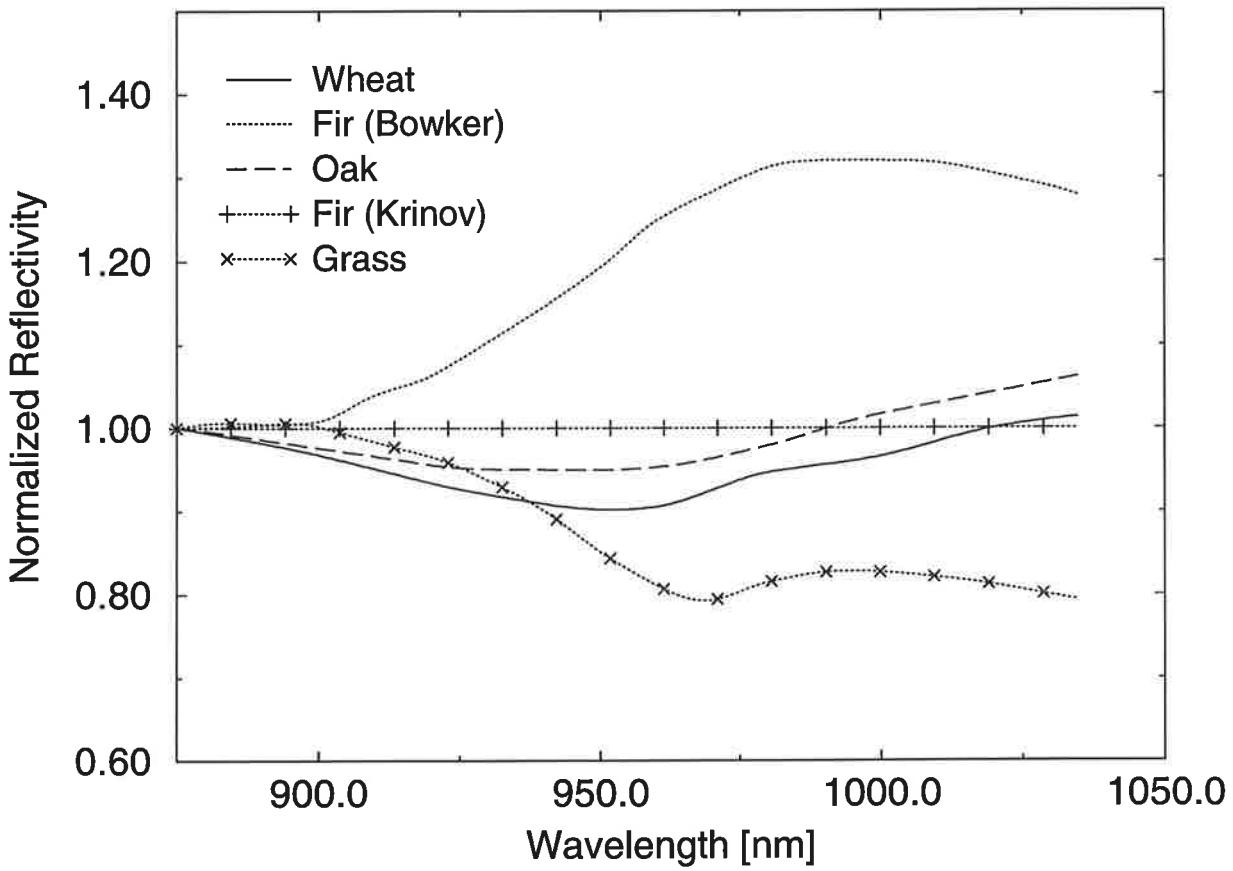
Wheat
Fir (Bowker)
Oak
Fir (Krinov)
Grass
1.40
1.20
1.00
0.80
0.60
Normalized Reflectivity
900.0
950.0
1000.0
1050.0
Wavelength [nm]

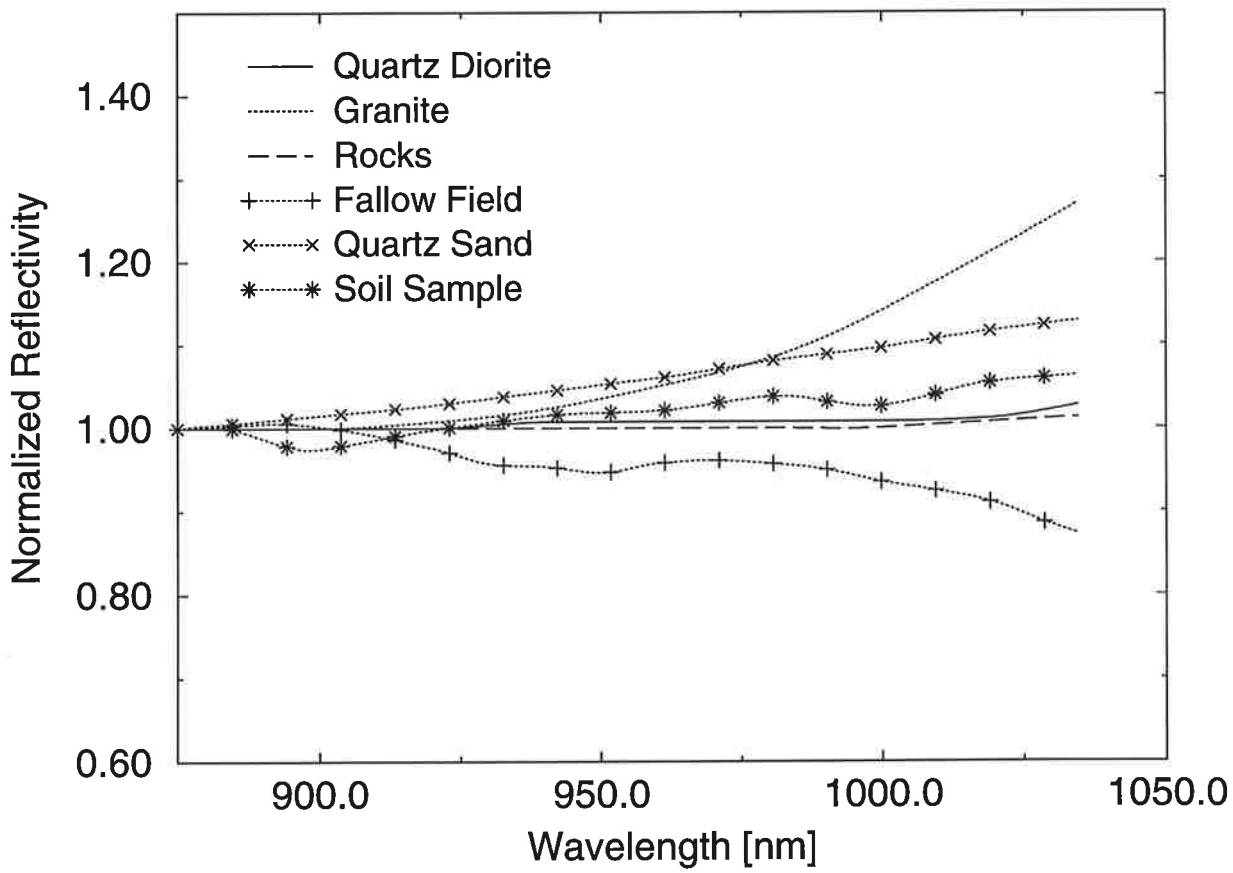
Quartz Diorite
Granite
Rocks
Fallow Field
Quartz Sand
Soil Sample
Normalized Reflectivity
1.40
1.20
1.00
0.80
0.60
900.0
950.0
1000.0
1050.0
Wavelength [nm]

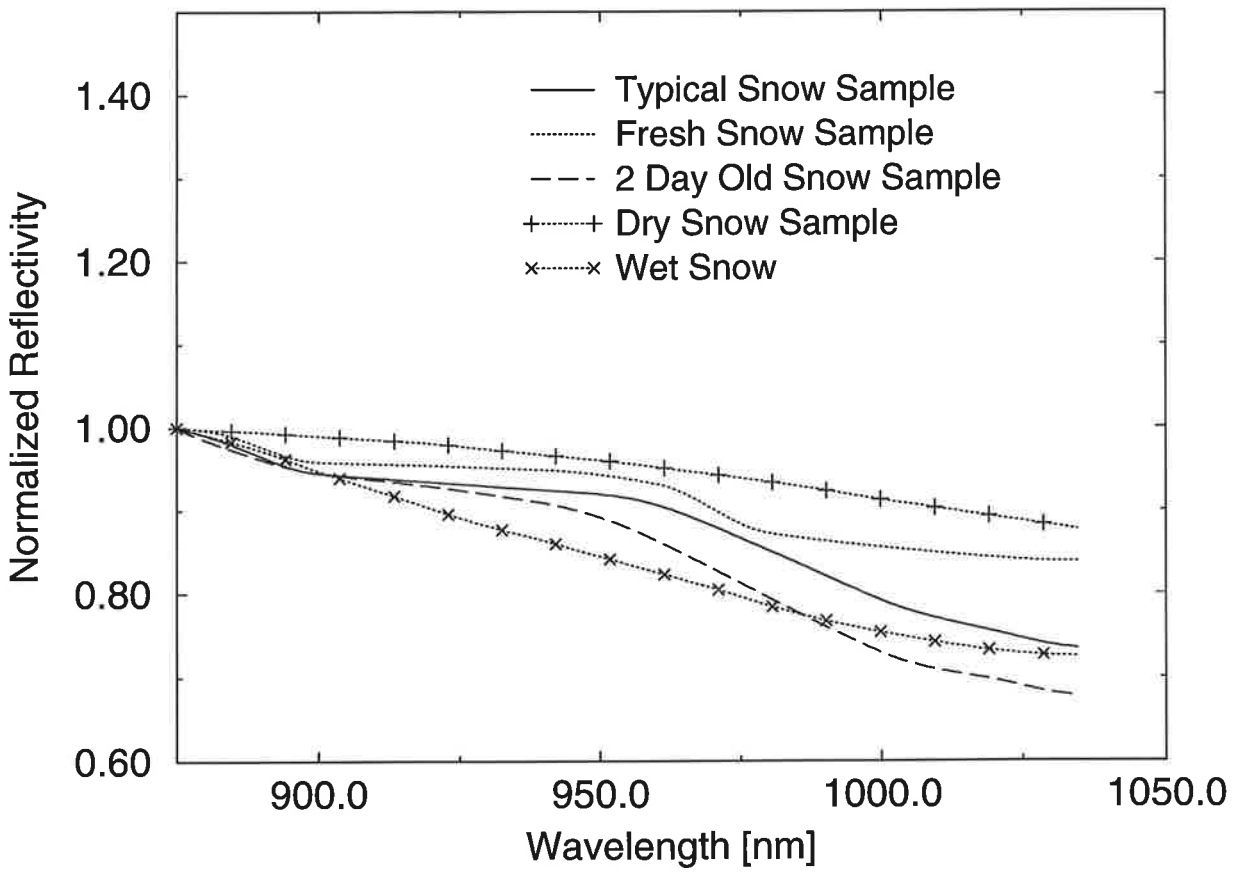
Typical Snow Sample
Fresh Snow Sample
2 Day Old Snow Sample
Dry Snow Sample
Wet Snow
Normalized Reflectivity
1.40
1.20
1.00
0.80
0.60
900.0
950.0
1000.0
1050.0
Wavelength [nm]

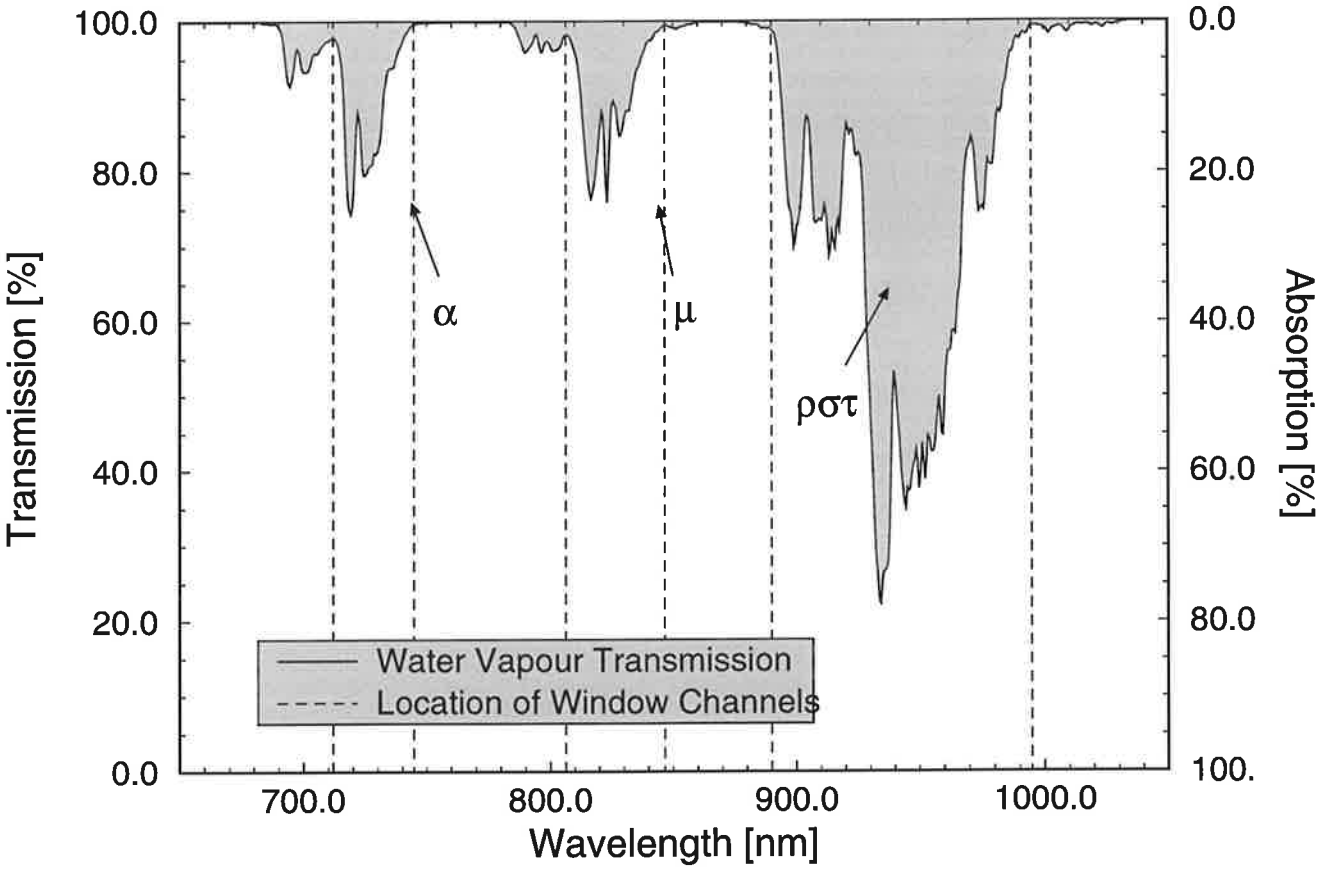
100.0
80.0
60.0
40.0
20.0
0.0
Transmission [%]
0.0
20.0
40.0
60.0
80.0
100.
Absorption [%]
α
μ
ρστ
Water Vapour Transmission
Location of Window Channels
700.0
800.0
900.0
1000.0
Wavelength [nm]

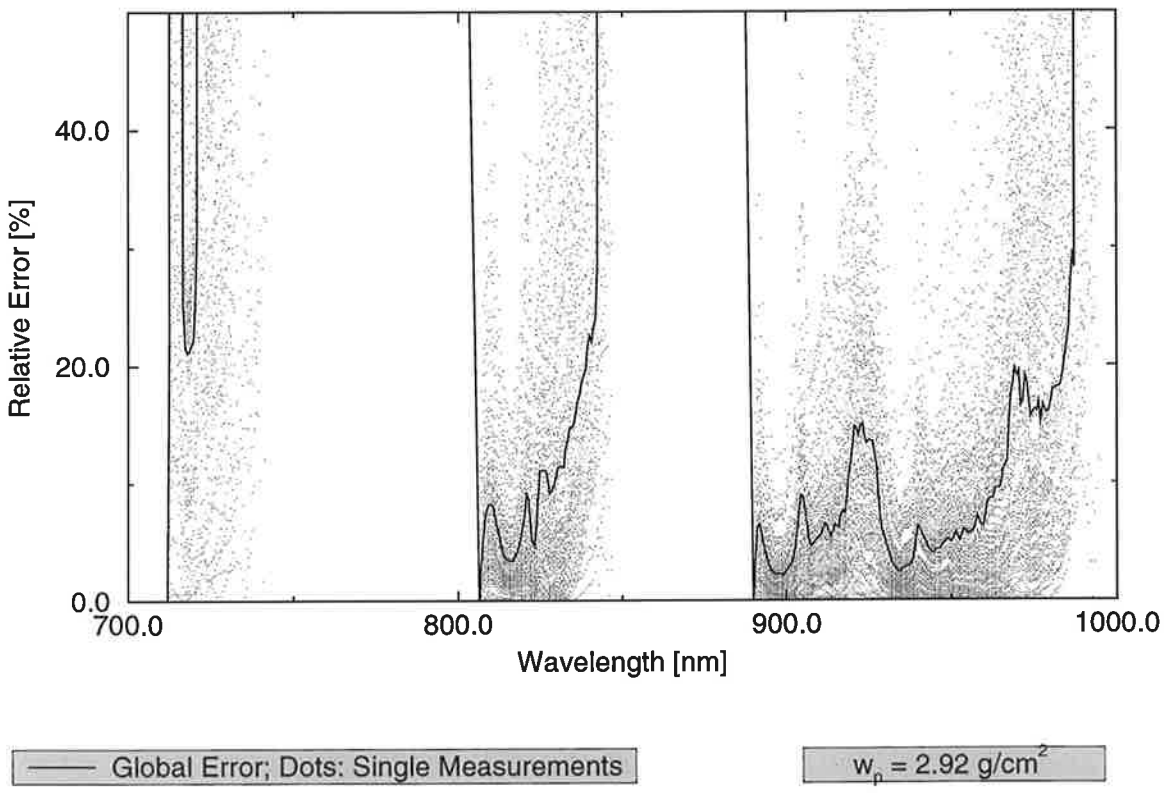
40.0
20.0
0.0
Relative Error [%]
700.0
800.0
900.0
1000.0
Wavelength [nm]
Global Error; Dots: Single Measurements
w_p = 2.92 g/cm^2

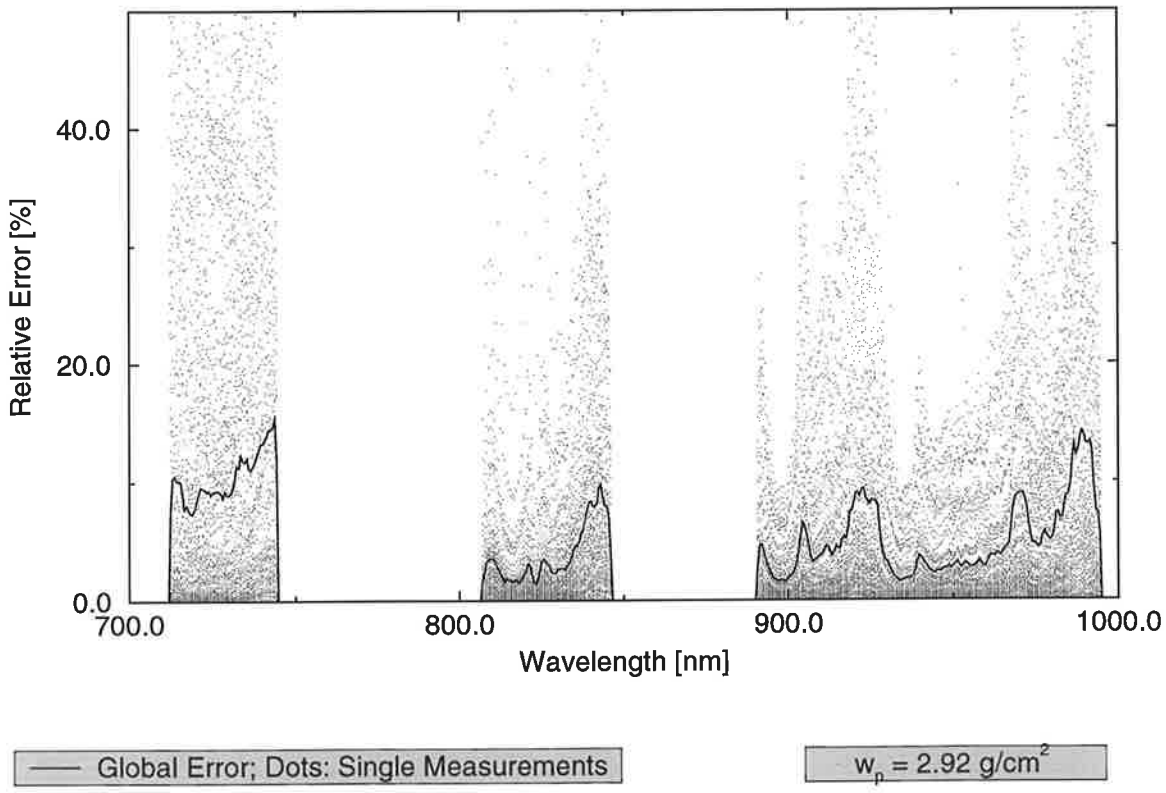
40.0
20.0
0.0
Relative Error [%]
700.0
800.0
900.0
1000.0
Wavelength [nm]
Global Error; Dots: Single Measurements
w_p = 2.92 g/cm^2

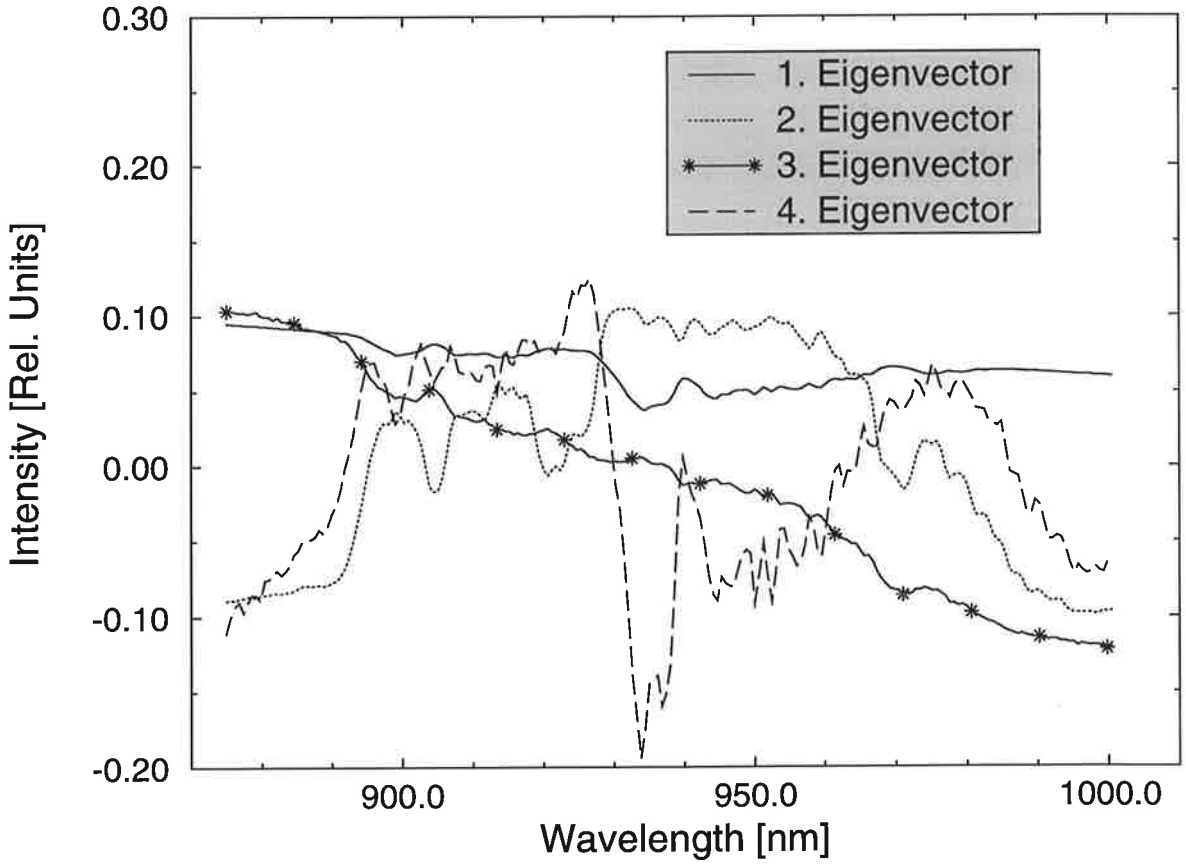
0.30
0.20
0.10
0.00
-0.10
-0.20
Intensity [Rel. Units]
900.0
950.0
1000.0
Wavelength [nm]
1. Eigenvector
2. Eigenvector
3. Eigenvector
4. Eigenvector

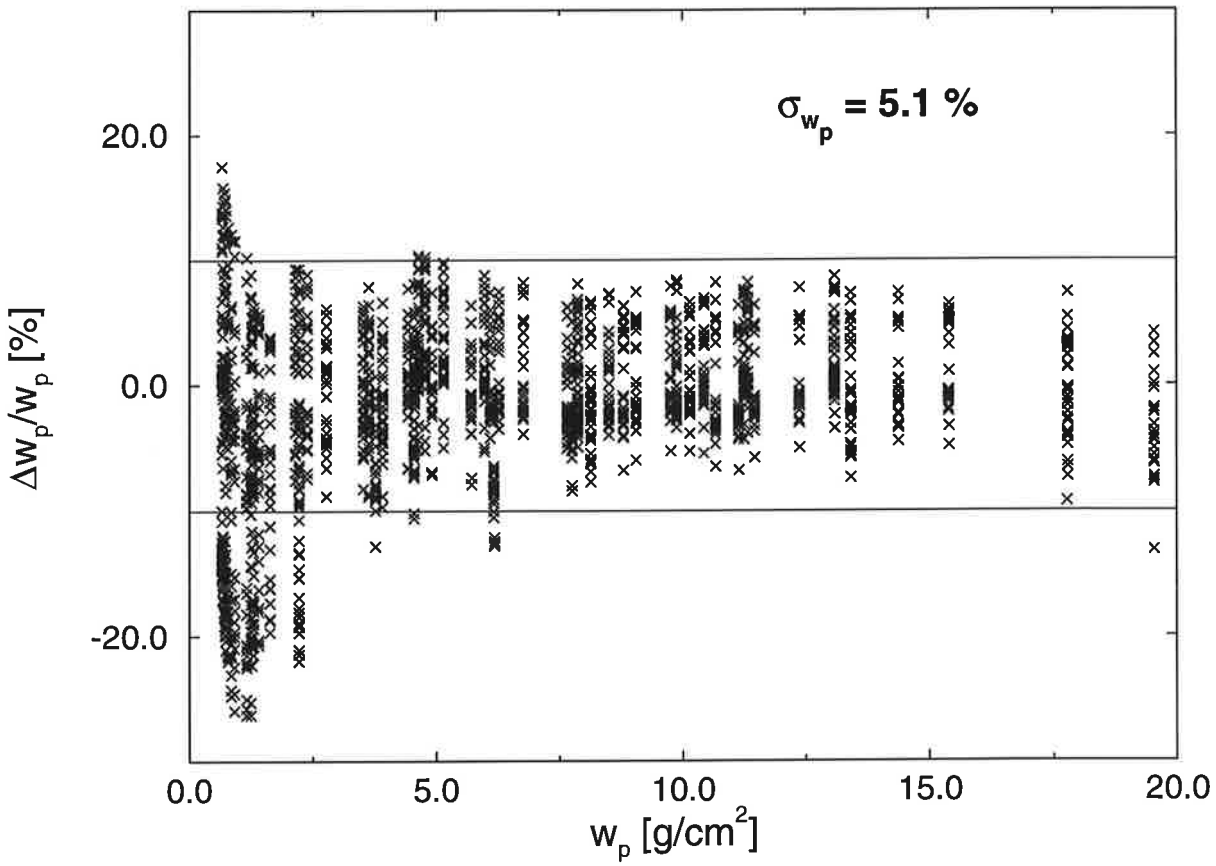
σ_{w_p} = 5.1 %
20.0
0.0
-20.0
$\Delta w_p/w_p$ [%]
0.0
5.0
10.0
15.0
20.0
w_p [g/cm^2]

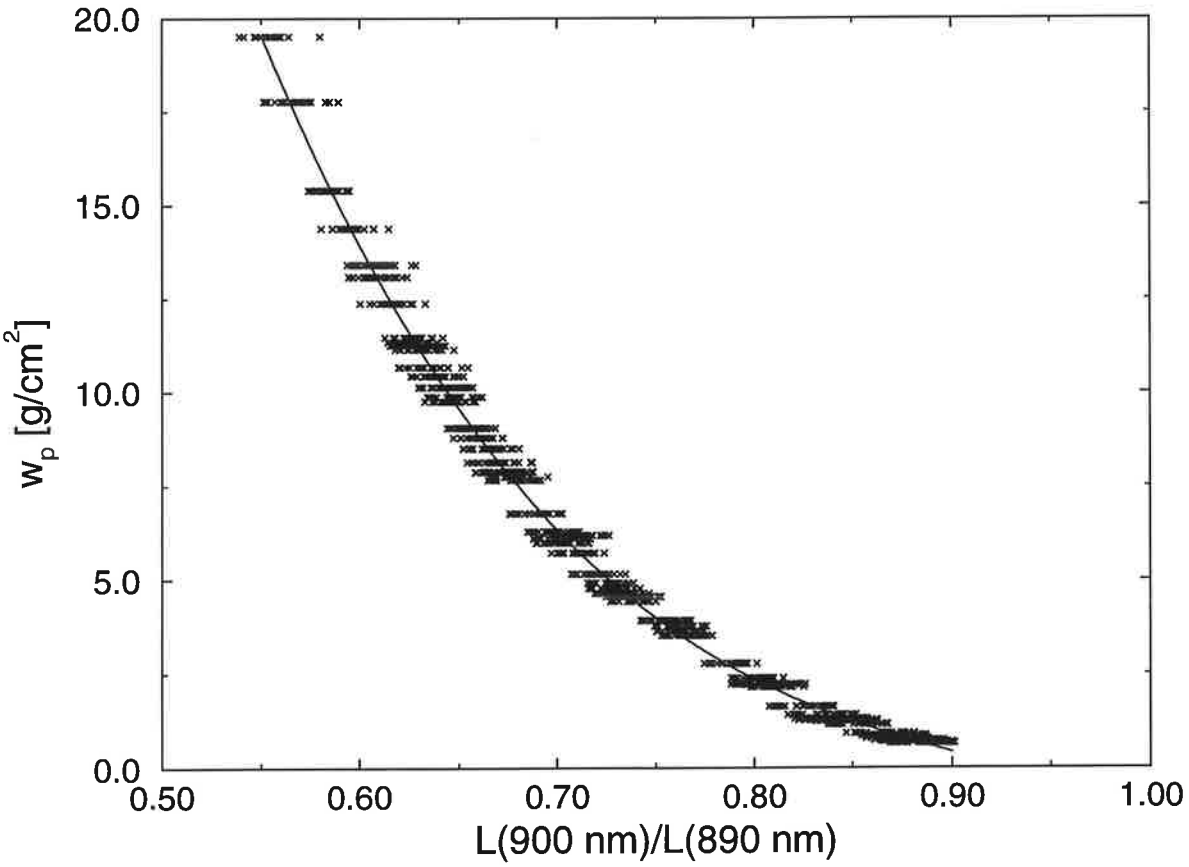
20.0
15.0
10.0
5.0
0.0
0.50
0.60
0.70
0.80
0.90
1.00
w_p [g/cm^2]
L(900 nm)/L(890 nm)

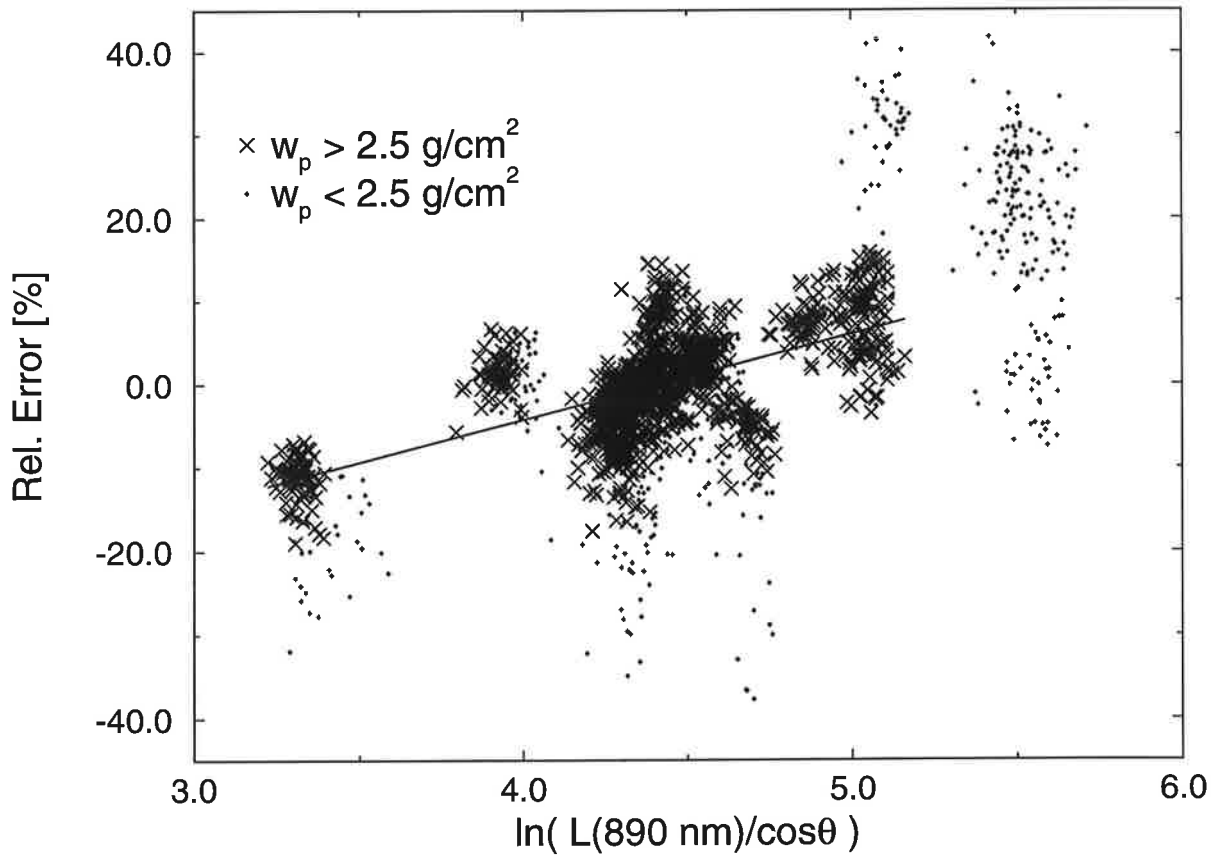
40.0
20.0
0.0
-20.0
-40.0
3.0
4.0
5.0
6.0
Rel. Error [%]
ln(L(890 nm)/cosθ)
× w_p > 2.5 g/cm^2
· w_p < 2.5 g/cm^2

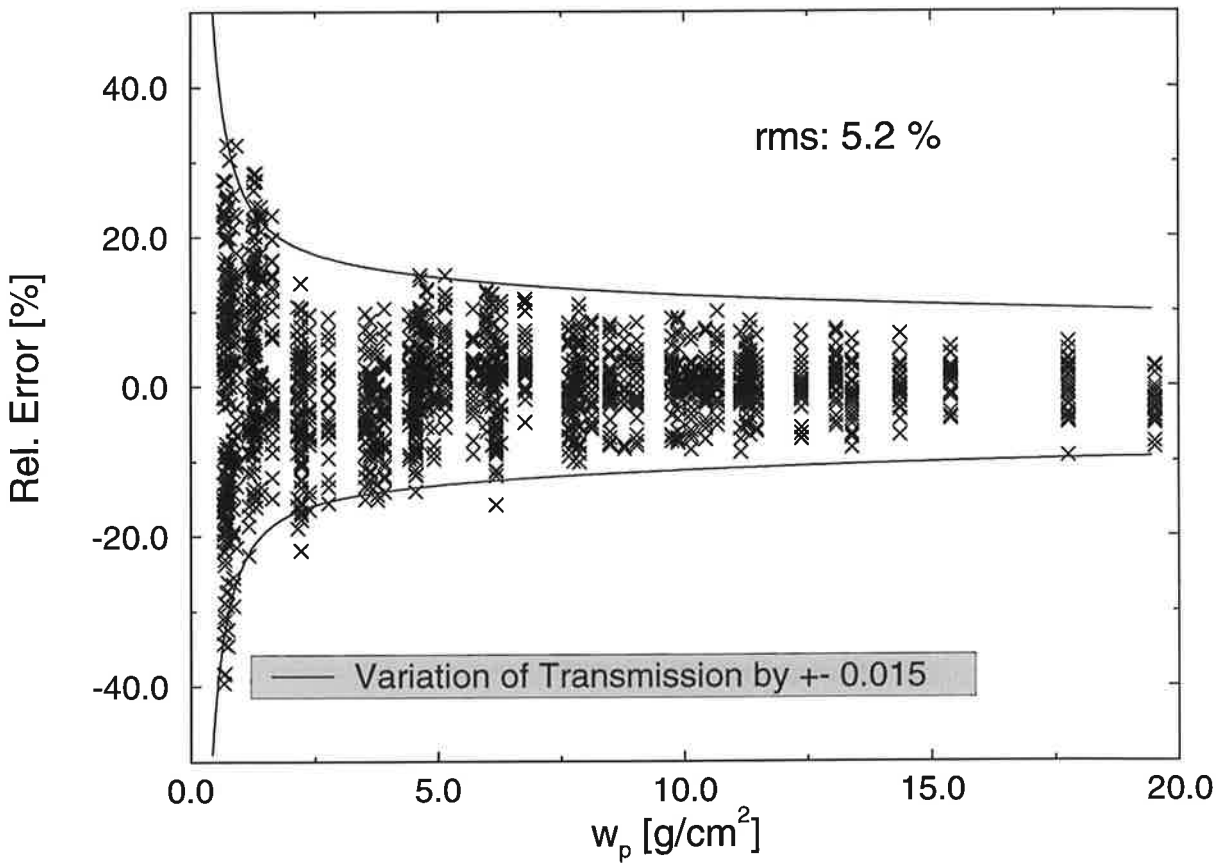
rms: 5.2 %
Variation of Transmission by +- 0.015
Rel. Error [%]
40.0
20.0
0.0
-20.0
-40.0
0.0
5.0
10.0
15.0
20.0
w_p [g/cm^2]

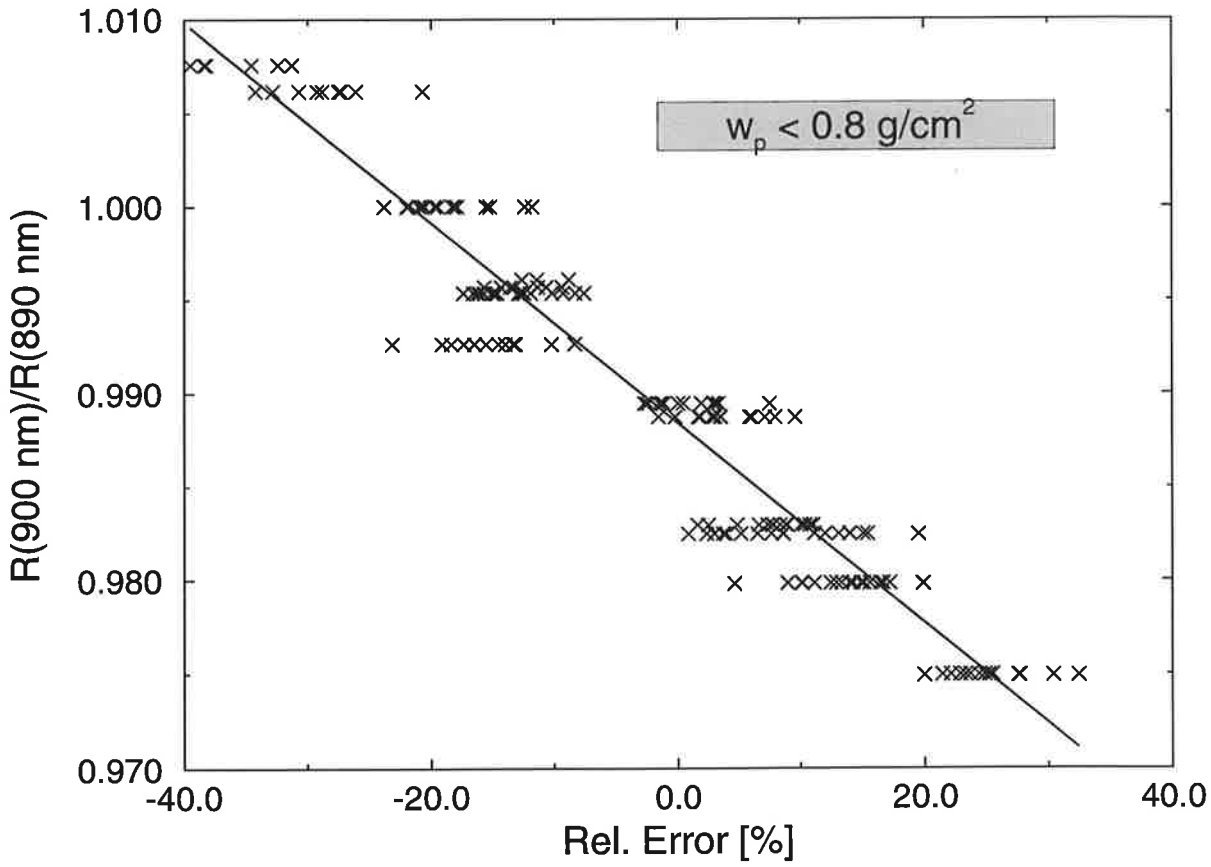
1.010
1.000
0.990
0.980
0.970
R(900 nm)/R(890 nm)
$w_p < 0.8$ g/cm^2
-40.0
-20.0
0.0
20.0
40.0
Rel. Error [%]

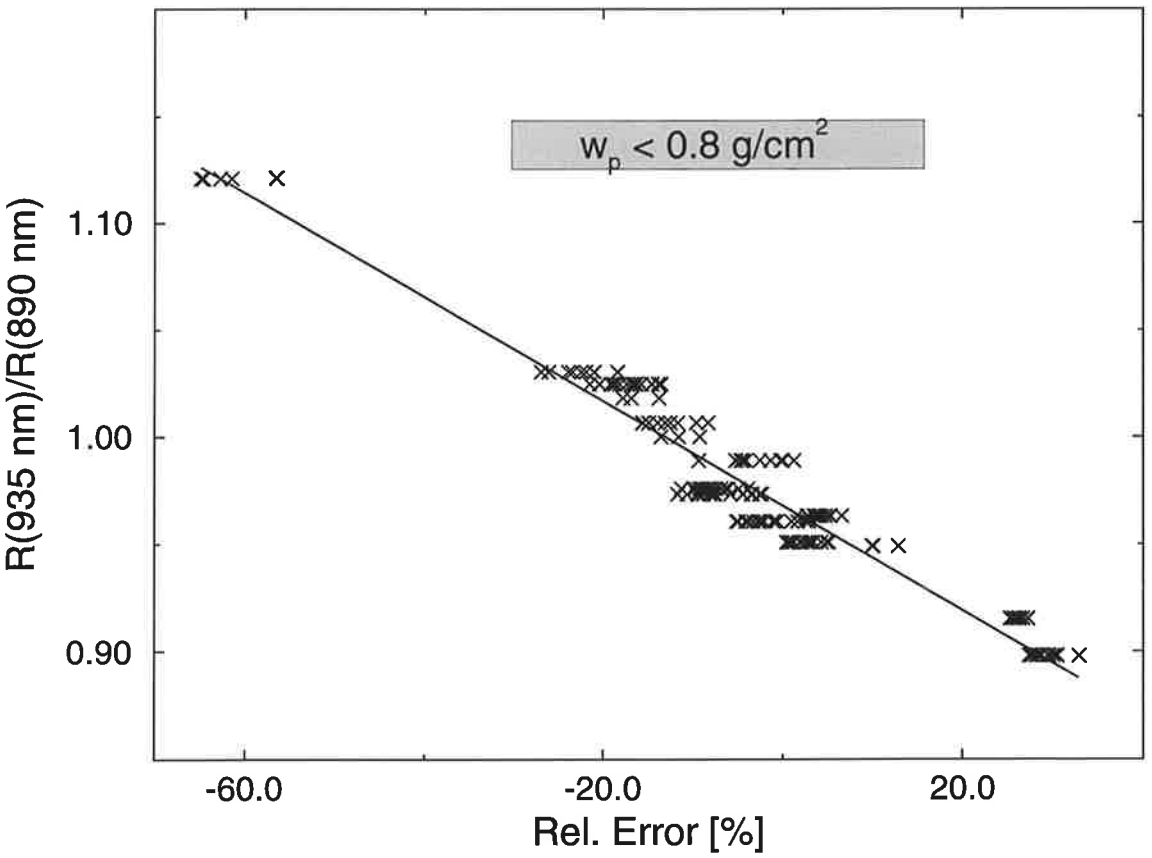
$w_p < 0.8$ g/cm^2
R(935 nm)/R(890 nm)
1.10
1.00
0.90
-60.0
-20.0
20.0
Rel. Error [%]

Passive Remote Sensing of Columnar Water Vapour Content above Land Surfaces:

Part II: Comparison of OVID Measurements with Radiosonde and DIAL Measurements

Barbara Bartsch, Meteorologisches Institut, Universität Hamburg, Germany

Stephan Bakan, Max-Planck-Institut für Meteorologie, Hamburg, Germany

Gerhard Ehret, Institut für Physik der Atmosphäre, DLR Oberpfaffenhofen, Germany

Jürgen Fischer, Institut für Weltraumwissenschaften, F. Universität Berlin, Germany

Martina Kästner, Institut für Physik der Atmosphäre, DLR Oberpfaffenhofen, Germany

Christoph Kiemle, Institut für Physik der Atmosphäre, DLR Oberpfaffenhofen, Germany

ISSN 0937-1060

Corresponding author: Dr. Stephan Bakan, Max-Planck-Institut für Meteorologie,
Bundesstrasse 55, D-20146 Hamburg, Germany, e-mail: bakan@dkrz.de

Abstract

Various efforts are currently being made to develop remote sensing techniques for high accuracy determination of atmospheric columnar water vapour content above land surfaces. Most of those algorithms are based on radiative transfer calculations, however, which have to be verified by spectral airborne or satellite measurements.

Initial verification of a new algorithm with the aid of airborne spectral data using the spectrometer OVID (**O**ptical **V**isible and near **I**nfrared **D**etector), an airborne water vapour DIAL (**Di**fferential **A**bsorption **L**idar), an aircraft humicap sensor and radiosonde data is performed during a flight experiment over Southern Germany. This water vapour algorithm is also dedicated to the MERIS (**ME**dium **R**esolution **I**maging **S**pectrometer) instrument on board ESA's satellite ENVISAT which will be launched 1999.

Spatial water vapour gradients of $\Delta H_2O = 0.1$ g/cm^2 over a distance of 100 km were resolved by applying the OVID measurements. The error estimation of the absolute value of the retrieved water vapour contents poses some problems due to insufficient additional temporal and spatial radiosonde data. However, the principal feasibility has been proven.

1. Introduction

Global fields of atmospheric water vapour are an important prerequisite for numerical weather prediction and climate studies. Satellites are the ideal platforms to provide such fields with the required spatial and temporal coverage. Although the derivation of detailed vertical profiles is still out of scope, total and boundary layer water vapour columns over the ocean may be calculated from microwave data (Schulz et al. 1993). However, over land these procedures do not provide sufficient accuracy.

Existing water vapour measuring techniques using satellite based instruments are subject to errors of more than 20% compared to in-situ measurements. These techniques are based on microwave or thermal infrared measurements which are strongly influenced by the highly variable surface emissivity.

Alternatively, the use of the backscattered solar radiation in the near infrared has been studied where various strong water vapour absorption bands exist. Although surface reflectivity is also highly variable in the considered spectral region, an initial approach shows that water vapour can be derived more accurately (Fischer 1989; Frouin et al. 1990; Gao et al. 1993).

Bartsch and Fischer (1997) describe the development of a method for the MERIS instrument on board ESA's satellite ENVISAT, together with an overview of the accuracy of present satellite techniques. This companion paper is referred to by BF in the following. A first application of the algorithm to aircraft measurements is discussed in the present paper. The data were collected with the airborne spectral analyzer OVID (**O**ptical **V**isible and near **I**nfrared **D**etector), described in section 3, during the aircraft measurement campaign CIVEX'95 (see section 2).

A DIAL which measures vertical profiles of the atmospheric water vapour content for an atmospheric layer with a maximum thickness of about 3000 m was installed on board the aircraft (section 4). Those data are used for comparison of the total water vapour values retrieved from the OVID measurements.

In section 6 water vapour values derived from OVID data are described and compared to aircraft humicap measurements, radiosonde and DIAL data.

2. Airborne Measurements during CIVEX '95

a. The Aircraft Measurement Campaign CIVEX'95

The airborne measurement campaign CIVEX'95 (Cloud **I**nstrument **V**alidation **EX**periment) took place in Southern Germany from 4 to 23 May 1995 (Costanzo et al. 1996). It was carried out in close cooperation between the Universität Hamburg, Max-Planck-Institut für Meteorologie, Hamburg, Freie Universität Berlin, and the DLR (**D**eutsche Forschungsanstalt für **L**uft- und **R**aumfahrt) Institut für Physik der Atmosphäre, Oberpfaffenhofen. CIVEX'95 was focused on validation and further improvements of airborne and satellite methods for remote sensing of cloud top height, total atmospheric water vapour content, microphysical cloud parameters and radiative properties of clouds.

The measurements were performed on board the research aircraft FALCON 20 of the DLR, based at the Dornier airfield in Oberpfaffenhofen near Munich.

The multispectral sensor system OVID (section 3) and a water vapour DIAL system (section 4) have been installed for remote sensing. The data of these instruments are used within this study to test and validate the water vapour algorithm of BF. Humidity data from an on board standard humicap sensor and from several radiosonde stations were available for comparison and verification.

b. Measurements for Water Vapour Retrieval Studies

Several measurement flights were conducted during the campaign period; the flight on 23 May 1995 was especially well suited for the purpose of water vapour determination, due to the cloudless conductions and the availability of all relevant instruments.

Fig. 1 shows the experimental area, the flight track, and the location of radiosounding stations for additional comparison. The flight pattern was chosen in west-east direction between Kempten and Salzburg in Southern Germany at four different flight levels: 120 (3720 m msl), 220 (6845 m msl), 150 (4655 m msl) and 180 (5590 m msl).

On 23 May 1995 Southern Bavaria is influenced by a high pressure ridge resulting in mostly fair weather. The axis of the ridge is located between Munich and Stuttgart with a north to south orientation moving slowly eastwards. A cold front approaches from France, but does not reach Germany this morning. Munich therefore lies in the anti-cyclonic stream pattern of the ridge with descending vertical motion, while Stuttgart is in a weak cyclonic stream pattern in front of a trough with ascending air. The winds are weak and change from SE to SW during the morning in Munich and Stuttgart.

The radiosondes profiled at Munich and Stuttgart from 00 and 12 UTC exhibit a residual boundary layer which is sharply marked in the dew point temperature profiles (Fig. 2). A comparison of the 00 and 12 UTC profiles at Stuttgart indicates a remarkable lift of the boundary layer from 830 to 750 hPa, corresponding to about 800 m. The radiosondes at Sigmaringen also show this upward motion of the boundary layer. On the other hand, the Munich profiles reveal the boundary layer descending weakly by about 250 m.

The boundary layer is characterized by a dry air mass. The differences in mixing ratios, dew points, and visibility between Munich and Stuttgart are not very pronounced, so that it can be assumed that the same air mass with similar properties is in Stuttgart and Munich. The thickness of the boundary layer is thus directly related to the water vapor content, which shows a gradient from west to east. This situation provides favourable circumstances for water vapour retrieval under different conditions.

3. Water Vapour Retrieval with the Spectrometer OVID

a. Technical Data

OVID – **O**ptical **V**isible and near **I**nfrared **D**etector – is a multichannel spectral analyzing instrument for atmospheric sensing (Armbruster et al. 1994; Bartsch and Bakan 1993). Two separate but almost identical detector units are used to cover the maximum possible spectral ranges of 0.25 to 1.05 µm (VIS) and 1.0 to 1.65 µm (NIR), which is reduced in praxis by the selected gratings of the spectrograph. Fig. 3 shows the schematic structure of one detector system of OVID. It consists of a mirror telescope, focusing the incoming radiation to a bundle of fibre cables connected with

the spectrograph in front of the thermo-electrically cooled detector. Normally, short fibre cables with only small absorption features are used. However, the limited space on board the FALCON 20 aircraft meant that during CIVEX '95 fibre cables of 10 m length had to be used. These unfortunately have a strong absorption band which increases the measurement error of the spectral data between 0.93 and 0.98 μm. Nevertheless, this has no influence on the value of the acquired data, as the proposed algorithm for water vapour determination does not require this spectral range.

The short-wave detector consists of a two-dimensional CCD array with 1024 x 256 pixels at 14 bit resolution. The wavelength axis is aligned with the longer array size so that 1024 wavelengths can be measured simultaneously. For each wavelength the signal can be integrated from 1 to 256 pixels in the other array direction, giving a wide range of detectable intensities and improving the signal-to-noise ratio. During CIVEX '95 radiance measurements were possible between 0.74 and 1.03 μm, thanks to a grating of 600 lines/mm and an appropriate optical filter to avoid second order spectral signals. The spectral resolution was 0.73 nm.

While the minimum exposure time for one spectrum is approximately 40 ms, the exposure time for our measurements had to be adjusted to the scene brightness. It was chosen between 100 and 200 ms, corresponding to sampling rates between 5 and 10 Hz. The number of integrated pixels per wavelength was also varied to adjust to different intensity levels of the detected signals.

The near infrared InGaAs detector consists of one diode array with 256 pixels at 14 bit resolution for the spectral range 1.0 and 1.65 μm with a spectral resolution of about 10 nm. However, only the VIS detector unit was used for the water vapour remote sensing study of the present paper.

The technical data of OVID are summarized in Table 1.

b. Determination of Total Water Vapour Content with OVID

The algorithm used to determine the water vapour content beneath the aircraft with the aid of spectral measurements with the VIS unit of OVID is described in detail in BF. The water vapour path $w_{p,c,o}$ is determined by combination of a two stage regression and a correction factor for different surface elevations H. It represents the integrated water vapour column on the slant path of the solar rays from the top of the atmosphere to the surface and vertically back to the aircraft.

Only four input parameters are needed for water vapour retrieval:

- L(890 nm): The vertically backscattered solar radiance at 890.1 nm wavelength, the window or reference channel
- L(900 nm): The vertically backscattered solar radiance at 900.3 nm wavelength, the absorption channel
- H: The topographic height of the measurement area beneath the aircraft, and
- θ: The solar zenith angle at the measurement time

Defining the ratio

$$T: = L(900.3nm) / L(890.1nm) \tag{1}$$

the water vapour path $w_{p,c,o}$ is determined by the following three equations (2) to (4):

$$w_p = 224.3 - 697.0 \cdot T + 735.7 \cdot T^2 - 264.0 \cdot T^3 \quad , \quad w_p \; in \; [g/(cm^2)] \tag{2}$$

$$w_{p,c} = \frac{w_p}{0.549 + 0.102 \cdot \ln \frac{L(890.1nm)}{\cos\theta}} \tag{3}$$

These two regressions are sufficient for surface elevations equal to mean sea level, that means $w_{p,c,o} = w_{p,c}$. The rms error of the derived water vapour content has been found to be 5.2%.

The following correction to the derived water vapour content should be applied for surface elevations other than mean sea level:

$$w_{p,c,o} = \frac{w_{p,c}}{a_o + a_1 \cdot H + a_2 \cdot H^2} \tag{4}$$

The correction factors for surface elevations between 350 and 850 m above msl and a midlatitude

summer atmosphere are given by a_0 =0.9758, a_1 =3.7373e-5 m^{-1}, a_2 =-9.8125e-08 m^{-2}. The remaining error of the retrieved water vapour content induced by variable surface elevation is about 0.5%.

For spaceborne measurement the columnar water vapour w can be derived from the water path $w_{p,c,o}$ of Eq. (4) by

$$w = \frac{w_{p,c,o}}{1 + \frac{1}{\cos\theta}} . \tag{5}$$

For aircraft measurements the situation is slightly different. If w_k denotes the columnar water vapour above the aircraft, then the columnar water vapour w below the aircraft is derived by

$$w = \frac{w_{p,c,o} - \frac{w_k}{\cos\theta}}{1 + \frac{1}{\cos\theta}} \tag{6}$$

4. Water Vapour Retrieval with the DIAL System

a. The Differential-Absorption LIDAR Principle

The differential-absorption LIDAR technique applied in the near infrared can be used to measure range-resolved water vapour profiles. Measurements are performed at two wavelengths, one at the line center (on-line) and one on the wing (off-line) of an appropriate water vapour absorption line. The mean water vapour molecular number density, $\overline{N}(R)$, from the range cell $\Delta R = R_2 - R_1$ at distance $R = R_1 + \Delta R/2$ can be calculated with the well known DIAL equation approximation (Schotland 1974):

$$\overline{N}(R) = \frac{1}{2*\sigma*\Delta R} * \ln\left(\frac{P_{off}(R_2) * P_{on}(R_1)}{P_{on}(R_2) * P_{off}(R_1)}\right) . \tag{7}$$

In this equation, P_{on} and P_{off} correspond to the power received from the on-line and off-line wavelengths at distances R_1 and R_2, respectively. $\sigma = \sigma_{on} - \sigma_{off}$ is the molecular differential absorption cross section of the selected water vapour line, which can be determined via a Voigt profile calculation using known line parameters. When temperature insensitive lines are used this calculation can be performed with known temperature and pressure profiles taken from climatological studies (Browell et al. 1991). The absorption cross section for a DIAL laser with high spectral purity and a line width much smaller than the water vapour line width is given by $\sigma(\nu_0)$ where ν_0 denotes the wavenumber of the absorption line center.

b. The DIAL System of the DLR

The DLR DIAL uses a narrow-band tunable dye laser with sequential generation of the on-line and off-line wavelengths. It is pumped by a frequency-doubled Nd:YAG laser. The Nd:YAG laser operates in a Q-switched mode to provide short pulses with a repetition rate of 9 Hz. The dye solution Pyridine 1 in methanol contained in a flow cell enables sufficient laser output from the tunable laser system in the near-infrared at 720 nm. There are several water vapour lines in this wavelength region which are suitable for water vapour DIAL measurements in the PBL (Grossmann and Browell 1989a and b). On board the aircraft the wavelength of the narrow-band dye laser can be precisely adjusted to the line center of a selected water vapour line using the absorption spectra of a photo-acoustic cell at low water vapour pressure. The laser bandwidth and its wavelength stability are controlled by a Fizeau spectrometer and recorded by the data acquisition system for each shot-pair.

The airborne system's receiver consists of a 35-cm diameter Cassegrain telescope which collects the photons backscattered from the atmosphere. The photons passing the receiver optics are detected with a photomultiplier. A three-cavity interference filter is placed in the receiver channel to filter out the unwanted daytime background radiation. The resulting signal is then digitized with a resolution of 12 bits at a sampling rate of 20 MHz for each laser shot. The off- and on-line LIDAR signals are transmitted at a frequency of approximately 4.5 Hz, and the backscattered signals are sampled from a selected vertical range. A real-time microcomputer which controls the data acquisition system stores these data on a removable cartridge disk for further data processing on the ground. The most important system parameters are summarized in Table 2.

c. Calculation of the Effective Absorption Cross Section

In the system used, the spectral purity of the dye laser is not sufficient and the determination of σ is more complex. Careful analysis of the spectral profile of the DIAL laser has shown that the narrow-band laser line is accompanied by additional background emission (Ehret et al. 1993). The laser line profile cannot therefore be treated as an ideal monochromatic profile and the spectral behaviour has to be accounted for in Eq. (7). This is realized by introducing an effective differential absorption cross section

$$\sigma_{eff} = \frac{\int_0^\infty \sigma(\nu)\,[L(\nu-\nu_{on}) - L(\nu-\nu_{off})]\,d\nu}{\int_0^\infty L(\nu)\,d\nu}, \qquad (8)$$

where ν is the wavenumber in cm^{-1}, $L(\nu)$ is a normalized function which describes the spectral profile of the laser, ν_{on} and ν_{off} indicate the wavenumber of the line center and wing measurements, and $\sigma(\nu)$ represents the Voigt line profile.

The introduction of σ_{eff}, however, leads to another error source in the DIAL retrieval. It arises from the fact that the on-line laser spectrum is changed by the water vapour absorption. The narrow-band part of the on-line laser spectrum, which lies in the absorption line center, is much more attenuated than the background radiation in the line wings. This causes a deformation of the laser line spectral profile $L(\nu - \nu_{on})$ as a function of distance along the laser beam path.

This effect leads to a systematic underestimation of the water vapour concentration when using the unmodified laser line profile in Eq. (8) to calculate σ_{eff}. The error depends on the two-way optical depth of the probed atmosphere which itself is a function of the selected line strength and the water vapour number density. At optical depths < 0.3, typical only of limited ranges or very dry regions in the upper troposphere, the modification of the spectral profile is negligible (Ehret et al. 1993). The effective absorption cross section σ_{eff} for measurements in the PBL at optical depths > 0.3 has to be recalculated using the deformed laser line profile. An iterative correction procedure is applied to account for this range dependent effect. The laser line profile for these cal-

culations is modeled by an absorbed narrow-band laser peak and non-absorbed broad-band radiation. The bandwidth of the narrow-band part is measured by the Fizeau spectrometer mentioned above. The contribution of broad-band laser radiation can be uniquely determined from a line comparison, which means, that the vertical water vapour profiles measured with different strong absorption lines over the same atmospheric region are compared. Only one unique laser line spectral profile will match the two water vapour profiles.

The systematic error induced to water vapour calculations by the line comparison depends on the homogeneity of the atmosphere. In the case presented here it is about 10%.

5. Determination of Total Water Vapour

a. General Remarks

The proposed MERIS water vapour algorithm is applied to airborne data collected in a cloudless situation during of CIVEX 1995 (see section 2).

In order to adapt the narrow-band measurements to the detector function defined in BF, a weighting average was applied to the spectral radiance measured, yielding the demanded detection bandwidth of 10 nm. The prescribed center wavelengths of 890.1 and 900.3 nm were obtained by spectral interpolation of the high-resolution data.

Water surfaces had to be excluded from further analysis by the following threshold condition for the minimum window channel radiance at 890.1 nm normalized to vertical incidence

$$L(890.1nm)/\cos\theta > 30W/(m^2 sr\ \mu m)\ . \qquad (9)$$

This accounts for the fact that the algorithm is so far only valid for land but not for water surfaces.

In order to account for changes in water vapour transmission due to finite surface elevations by Eq. (4), the LIDAR data are used to determine the surface elevation H beneath the flight track.

b. Columnar Water Vapour Content beneath Flight Level 120

The retrieved total water vapour content beneath flight level 120, using the proposed surface elevation corrected algorithm for the OVID data, is shown in Fig. 4. Individual data points represent averages over 34 single water vapour values of OVID, in order to match the spatial resolution of the DIAL measurements. The data are restricted to the area east of 11.5°E, where no average spatial trend for the water vapour column prevailed (as can be seen from Fig. 7). Data variability in this area is found to show almost linear correlation with surface elevation.

The derived water vapour column values correspond in general to data from other sources. Causes for the differences to some of the radiosoundings will be discussed later. The variability of the linearized trend with surface elevation may be attributed to various noise components. Therefore, the percentage deviation of the individual values from the linear regression of Fig. 4 is presented in Fig. 5. The maximum deviations of the non averaged values from the linear regression are about 15% with only a few exceptions. Only 0.7 to 1.5% deviation can be explained with measurement noise of OVID. The conclusion is therefore that these errors are mainly induced by variable spectral surface reflectivity.

This 15% deviation coincides closely with the maximum error influence of different surfaces derived from simulations with nearly the same water vapour path w_p, which is described in detail in BF. This suggests that the variety of spectral surface reflectance values is reasonably well chosen within the simulations.

Fig. 4 also shows the total water vapour column calculated from the FALCON humicap measurements during the final descent to the airbase at Oberpfaffenhofen. The error bar indicates accuracy limits of ± 5% due to an accuracy estimate of 2% for ground based operation of the FALCON humidity sensor (Fimpel 1997) and 5% for inflight operation (Busen 1996). Comparison with the values collected during the ascent of the aircraft show that the columnar water vapour content between 140 m agl (start height of recording during ascent) and flight level 220 differs only by about 4%, so that temporal changes can be neglected. The column water vapour content retrieved by the FALCON humicap measurements is around 3.6% smaller than that retrieved from the OVID data, indicating satisfactory coincidence.

There are greater deviations between the radiosonde measurements at Munich at 0 and 12 UTC, Sigmaringen at 7 and 13 UTC, and Stuttgart at 0 and 12 UTC (Deutscher Wetterdienst 1995). The humidity soundings were interpolated to the flight time and vertically integrated. Table 3 contains the deviations of these time interpolated water vapour contents from those retrieved from OVID measurements. The water vapour values from the radiosondes are between 13.1 and 19.9% (between 0.13 and 0.19 g/cm^2) lower than those from OVID data. As the accuracy of the radiosondes is around 0.11 g/cm^2 (Hoehne 1980), these deviations are greater than expected. This may arise from the insufficient spatial and temporal collocation of the different instruments and from remaining inaccuracies in water vapour absorption derived from theoretical calculations. Measurement errors of the spectrometer OVID can only explain deviations of up to 3% (noise: 0.3% for the average water vapour values, systematic measurement errors: 2.6%). The rms error of the used algorithm is stated to be 5.2% in BF.

c. Investigation of other flight levels

Fig. 6 shows the linear regressions of the retrieved water vapour content below the four flight levels in comparison with the FALCON humicap measurements between 11°30'E and 12°05'E. The FALCON humicap and the OVID measurements coincide closely (deviation between 3.8 and 5.2%) except for the measurements at flight level 150, where a 10% deviation between FALCON humicap and OVID measurements is observed. This points to a water vapour gradient towards the north, where the measurements for flight level 150 were taken.

The FALCON humicap measurements are height integrated values of the water vapour content. The greatest influence on these measurements is exerted by the surface values of the water vapour content measured during take-off and landing at the Oberpfaffenhofen airport. It is therefore not possible to resolve spatial gradients of the columnar water vapour content with the FALCON humicap measurements.

d. Measurement of Spatial Water Vapour Distributions

In accordance with the mentioned moisture gradient in the experiment area (section 2.a) a 10 to 15% change in water vapour column is found in east-west direction. Fig. 7 shows the smoothed deviation of water vapour content corrected to surface elevation by use of the linear regressions of

the east-legs shown in Fig. 6 for the flight levels 150 and 220 in dependence of longitude. For the other flight levels, either no surface elevation data exist for the western flight leg (flight level 180) or the measurements started too far in the east (flight level 120) for comparison. In the western region total water vapour is about 10 to 15% higher than in the eastern region.

This also coincides with the DIAL backscatter measurements, which show a deeper boundary layer in the western part (Fig. 8). The measured height difference is about 400 m from west to east, accounting for the different orographic elevations. The thickness difference of 400 m corresponds to about 23% of the whole boundary layer, this dynamically explained change coincides well with the experimental data of OVID measurements as shown in Fig. 8.

These results indicate that changes of the water vapour column of at least 10% can be resolved by spectral airborne/satellite measurements.

d. Comparison with LIDAR Data

In a further step the water vapour retrievals from OVID and DIAL are compared here for the flight leg in flight level 120. However, several points have to be addressed before a meaningful comparison becomes possible:

OVID allows only to retrieve the integrated water vapour on the slant solar path from the top of the atmosphere to the surface and vertically back to the aircraft. No information about the vertical profile can be extracted. The water vapour content w_k above the aircraft has to be subtracted (see Eq. (6)) for comparison of the integrated water vapour below the aircraft. This is estimated by combining the aircraft humicap measurements with six radiosonde ascents. The errors introduced into the determination of the columnar water vapour content below the aircraft are small: The water vapour content above the aircraft for the comparison flight level 120 is estimated to be 0.107 ± 0.064 g/cm^2 from the aircraft humicap measurements between flight level 120 and 220 and above from the radiosonde ascents. Bearing the geometry of the solar path in mind (θ = 54.3°), the maximum error introduced to the total water vapour content below flight level 120 is 0.04 g/cm^2.

In contrast to OVID, the DIAL provides vertical profiles of the atmospheric water vapour below

the aircraft. However, the necessary averaging processes for noise reduction restrict these profiles to layers from 150 m above ground level (agl) to the point where the laser beam and telescope field of view begin to overlap. Therefore, vertical profiles for the flight leg in flight level 120, which corresponds to 3720 m msl, are only available for the layer from 150 m agl to 3000 m msl. That means that estimations of the water vapour content in the layers 0 to 150 m agl and 3000 m to 3720 m msl are also subtracted from the OVID results prior to comparison with the DIAL data. These estimates are derived from the integrated water vapour content of the FALCON humicap measurements during the final descent of the aircraft. Therefore, the water vapour columns retrieved from OVID data are reduced by 0.121 g/cm^2. This procedure is also consistent with the radiosonde data, interpolated to the OVID and LIDAR measurement time, which would suggest subtraction of values of 0.103 (Stuttgart), 0.105 (Munich), and 0.129 g/cm ^{2} (Sigmaringen), respectively. The corresponding error due to the estimation of the water vapour content between 0 and 150 m agl and between 3000 m and 3720 m msl might be less than 0.018 g/cm^2.

The DIAL was limited to a certain extent for water vapour retrieval from the moist boundary layer with low vertical extension on that particular day.

Fig. 9 shows a comparison of water vapour values in the layer from 150 m agl to 3000 m msl calculated from OVID, DIAL, radiosondes, and FALCON humicap measurements. Table 4 contains detailed analyses of the deviation in different measurements from the OVID retrieved values, with radiosonde values interpolated to aircraft measurement time.

The accuracy of the DIAL measurement for this flight is 15%. This is mainly due to the fact that significant heterogeneities were detected in the water vapour above 1500 m msl in both DIAL and radiosondes profiles. This introduces a 10% estimated uncertainty into the line comparison method necessary to obtain DIAL water vapour data (see section 4). An additional 5% uncertainty is due to noise. The accuracies of the radiosonde data are again 0.11 g/cm^2.

Table 4 shows a 30% gap between the DIAL and the OVID retrieved water vapour data. The FALCON humicap measurements coincide closely with the OVID data, whereas the radiosonde data lie between the DIAL and the OVID data (mean deviation of OVID measurements from radiosonde values: 21%; mean deviation of DIAL measurements from radiosonde values: 14%).

However, it is important to note that the radiosonde and the FALCON humicap measurements were carried out at least 50 km away from the OVID and DIAL measurements. Therefore, differences between data from these instruments and from OVID and DIAL measurements can partly be due to spatial water vapour gradients of up to 15%, which were also found by the OVID measurements (see Fig. 8).

Again, measurement errors of OVID can explain only up to 3% deviation. However, as already mentioned in the discussion of Fig. 4 and Table 3, the OVID water vapour retrieval algorithm is based on theoretical radiative transfer calculations which, in turn, use extensive spectral line data bases. As discussed in BF, faults in the HITRAN 1992 data base could also account for a considerable error.

Comparison between the two systems at higher flight levels is more difficult because the DIAL profiles are restricted to layers of about 3000 m thick below the aircraft. But as most of the columnar water vapour content is located in the boundary layer and dominates the OVID signal, profile corrections for meaningful comparison become more doubtful. A conceivable composition of vertical DIAL profiles from different flight levels requires either a very homogeneous weather situation or flight paths exactly above each other which is hardly possible in praxis. This is why comparison was restricted to the flight leg at flight level 120.

6. Discussion and Summary

The paper illustrates the first application of the water vapour algorithm described in BF to measured spectra. Spatial water vapour gradients of about 15% within the measurement area, coinciding with the dynamics of the weather situation, were successfully detected with the OVID spectrometer.

However, it is difficult to compare the derived integrated water vapour values of the different water vapour measuring instruments. The radiosonde measurements are carried out at least 50 km away from the measurement area. The time intervals are between half an hour and seven hours. Time deviations caused by the aircraft humicap measurements can be neglected because the integrated water vapour values derived during the ascent and the descent of the aircraft only vary by 4%.

On the other hand spatial water vapour differences of 10 to 15% are detected in the measurement area by the OVID measurements (section 5d). Unfortunately, most of the water vapour is located near the surface and thus the humicap measurements are more representative for the water vapour contents near the airport Oberpfaffenhofen than at the measurement area.

Comparison of different absorption lines in terms of the water vapour estimates from DIAL measurements was difficult due to the spatial heterogeneity detected in the water vapour.

It is therefore difficult to make an exact statement about the quality of the water vapour content retrieved by OVID. Retrieval errors may originate from the uncertainties of the absorption line parameters used for the algorithm development as described in BF.

In conclusion, further measurements are necessary for more accurate qualification of the water vapour algorithm. These measurements should be taken without temporal or spatial distances between the various measuring instruments.

However, if the evaluation of further measurements provides evidence of systematic inaccuracies in the algorithm, it is only necessary to adapt the coefficients of the algorithm to the correct absorption strength.

Finally, spectral measurements are strongly recommended as verification of algorithms based on theoretical radiative transfer calculations. This will help to establish an algorithm for retrieving water vapour contents from measurements of ESA's MERIS on board ENVISAT which will be launched in 1999.

Acknowledgements

This work was supported by the German BMBF (Bundesministerium für Bildung und Forschung) which enabled the acquisition of OVID via the project „Spektral hochauflösende Messungen rückgestreuter Strahlung über Wolken im Spektralbereich $\Delta\lambda$ = 0.2 - 4.5 μm". The measurement campaign CIVEX'95 was partly financed by the EU-project „Remote Sensing of Cloud Parameters from Multispectral Radiances in the Visible and Near Infrared". The radiosonde data are provided by the German Weather Service DWD.

REFERENCES

Armbruster, W., B. Bartsch, L. Schüller, S. Bakan, J. Fischer, 1994: OVID measurements during EUCREX'94, *EUCREX European Cloud and Radiation* Experiment, Seventh Workshop in Villeneuve d'Ascq, France, 13-15 September *1994*, ed. G. Brogniez, Laboratoire d'Optique Atmospheric, Villeneuve d'Ascq cedex, 47-55.

Bartsch, B. and J. Fischer, 1997: Passive Remote Sensing of Columnar Water Vapour Content above Land Surfaces, Part I: Theoretical Algorithm Development, submitted to *J. Appl. Meteor.*

Bartsch, B. and S. Bakan, 1993: Aircraft measurements: First experiences with the array spectrometer OVID, *Berichte aus dem Zentrum für Meeres- und Klimaforschung, Reihe A*, **11**, in „Arktis 1993, Report on the Field Phase with Examples of Measurements", ed. B. Brümmer, 147-156.

Browell, E. V., S. Ismail, and B. E. Grossmann, 1991: Temperature sensitivity of differential absorption lidar measurements of water vapor in the 720 nm region, *Appl. Opt.*, **30**, 1517-1524.

Brümmer, B., 1993: Arktis 1993, Report on the Field Phase with Examples of Measurements, *Berichte aus dem Zentrum für Meeres- und Klimaforschung, Reihe A*, **11**, pp. 186.

Busen, R., 1996: private communication.

Costanzo, C., S. Bakan, B. Bartsch, G. Ehret, J. Fischer, C. Kiemle, T. Kriebel, L. Schüller, P. Wendling, 1996: CIVEX'95 - Field Phase Report and First Results of Airborne Measurements for the EU-Project: „Remote Sensing of Cloud Parameters from Multispectral Radiances in the Visible and near Infrared", to be submitted in *Strahlung in Atmosphäre und Ozean, Beiträge zur Fernerkundung*, Freie Universität Berlin, Institut für Weltraumwissenschaften.

Deutscher Wetterdienst,1995: Europäischer Wetterbericht, *Amtsblatt des Deutschen Wetterdienstes, Aerologische Wettermeldungen*, Jahrgang 1, No. 143, pp. 4.

Ehret, G., C. Kiemle, W. Renger, and G. Simmet, 1993: Airborne remote sensing of tropospheric water vapor using a near infrared DIAL system, *Appl. Opt.*, **32**, 4534-4551.

Fischer, J., 1989: Clouds Satellite Observations: High Resolution Spectroscopy for Remote Sensing of Physical Cloud Properties and Water Vapour, *Current Problems in Atmospheric Radiation*, IRS'88, Lenoble and Geleyn (Eds.), 151-154.

Fimpel, H. P., 1987: The DFVLR Meteorological Research Aircraft FALCON-E: Instrumentation and Examples of Measured Data, Sixth Symposium on Meteorological Observations and Instrumentation, *January, 12-16, 1987*, New Orleans, AMS Boston, 113-116.

Frouin, R., P.-Y. Deschamps, and P. Lecomte, 1990: Determination from space of atmospheric total water vapour amounts by differential absorption near 940 nm: Theory and airborne verification, *Appl. Meteor.*, **29**, 448-460.

Gao, B.-C., A. F. H. Goetz, Ed R. Westwater, J. E. Conel, and R. O. Green, 1993: Possible near-IR channels for remote sensing precipitable water vapour from geostationary satellite platforms, *Appl. Meteor.*, **32**, 1791-1801.

Grossmann, B. E. and E. V. Browell, 1989a: Spectroscopy of water vapor in the 720 nm region: line strengths, self induced pressure broadenings and shifts, and temperature dependence of linewidths and shifts, *Mol. Spectrosc.*, **136**, 264-294.

Grossmann, B. E. and E. V. Browell, 1989b: Water vapor line broadening and shifting by air nitrogen, oxygen, and argon in the 720 nm wavelength region, *Mol. Spectrosc.*, **138**, 562-595.

Hoehne, W. E., 1980: Precision of National Weather Service upper air measurements, *NOAA Tech. Memo. NWS T&ED-16 [NTIS No. PB81-108136]*, NOAA National Weather Service, Sterling, VA, pp. 23.

Schotland, R. M., 1974: Errors in the lidar measurement of atmospheric gases by differential absorption, *Appl. Meteor.*, **13**, 315-331.

Schulz, J., P. Schlüssel, and H. Graßl, 1993: Water vapour in the atmospheric boundary layer over oceans from SSM/I measurements, *Int. J. Remote Sensing*, **14**, 2773-2789.

List of Figures

List of Tables

Table 1:

OVID System Parameters		
Detector/Spectrograph	VIS	NIR
Type	CCD	InGaAs diode array
Number of pixels	1024 x 256	256 x 1
Max. spectrum range	0.25 - 1.06 µm	1.0 - 1.65 µm
Effective aperture	3.8	2.0
Spectral resolution	0.43 - 1.7 nm	5.9 - 10 nm
Sample rates	5 - 10 Hz	5 - 10 Hz
Controller	VIS	NIR
A/D converter	14 bit	14 bit
Binning/grouping modus	+/+	-/-
Telescope	VIS	NIR
Mirror	Spherical	Spherical
Mirror diameter	8.0 cm	8.0 cm
Focal length	31.0 cm	16.0 cm
Viewing angle	0.3°	0.3°
Spatial Resolution	VIS	NIR
Perpendicular to flight direction at flight height 10000 m	47 m	60 m
Parallel to flight direction ($v_{aircraft}$ = 150 m/s):		
with exposure time	40 ms	100 ms
at flight height 10000 m	53 m	74 m

Table 2:

DIAL System Parameters	
Laser System	
Laser type:	Nd: YAG pumped dye-laser
Pulse width:	6 nsec
Pulse energy:	typ. 10 - 15 mJ, max. 30 mJ
Bandwidth:	≤ 0.03 cm^{-1} (FWHM)
Spectral purity:	typ. 70 - 75%
Repetition rate:	9 Hz
on-/off-line frequency:	4.5 Hz
Wavelength Control	
Wavelength calibration (on-line):	Water vapour filled PAS-cell
Precision:	0.01 cm^{-1}
Bandwidth control:	Fizeau type spectrometer
Spectral resolution:	0.007 cm^{-1}
Resolution of readout:	0.002 cm^{-1}/pixel
Receiver System	
Telescope:	35 cm Cassegrain
Spectral filter:	$\Delta\lambda = 0.65$ nm, 50% transmission
Detector:	Photomultiplier Hamamatsu R928
Electronic bandwidth of amplifier;	6 MHz
Digitizer:	12 bit 20 MHz
Data acquisition system:	PDP 11, Q-Bus, CAMAC
Storage medium:	Removable disk 88 Mbyte

Table 3:

Elevation	OVID	Radiosonde (R) or FALCON Humicap (F)			
Equal to	w [g/cm^2]	Type (R or F)	Distance [km]	w [g/cm^2]	Δw/w [%]
Sigmaringen	0.90	R	200 ± 20	0.76 ± 0.11	- 15.6
Munich	0.96	R	50 ± 10	0.77 ± 0.11	- 19.9
Stuttgart	1.03	R	230 ± 20	0.89 ± 0.11	- 13.1
Oberpfaffenhofen	0.92	F	50 ± 50	0.89 ± 0.04	- 3.6

Table 4:

Elevation	OVID	DIAL		Radiosonde (R) or FALCON Humicap (F)			
Equal to	w [g/cm^2]	w [g/cm^2]	Δw/w [%]	Type (R or F)	Distance [km]	w [g/cm^2]	Δw/w [%]
Sigmaringen	0.77	0.52 ± 0.08	- 32	R	200 ± 20	0.63 ± 0.11	- 18
Munich	0.84	0.60 ± 0.09	- 28	R	50 ± 10	0.67 ± 0.11	- 20
Stuttgart	0.91	0.67 ± 0.10	- 26	R	230 ± 20	0.79 ± 0.11	- 13
Oberpfaffen-hofen	0.80	0.55 ± 0.08	- 31	F	50 ± 50	0.78 ± 0.04	- 3

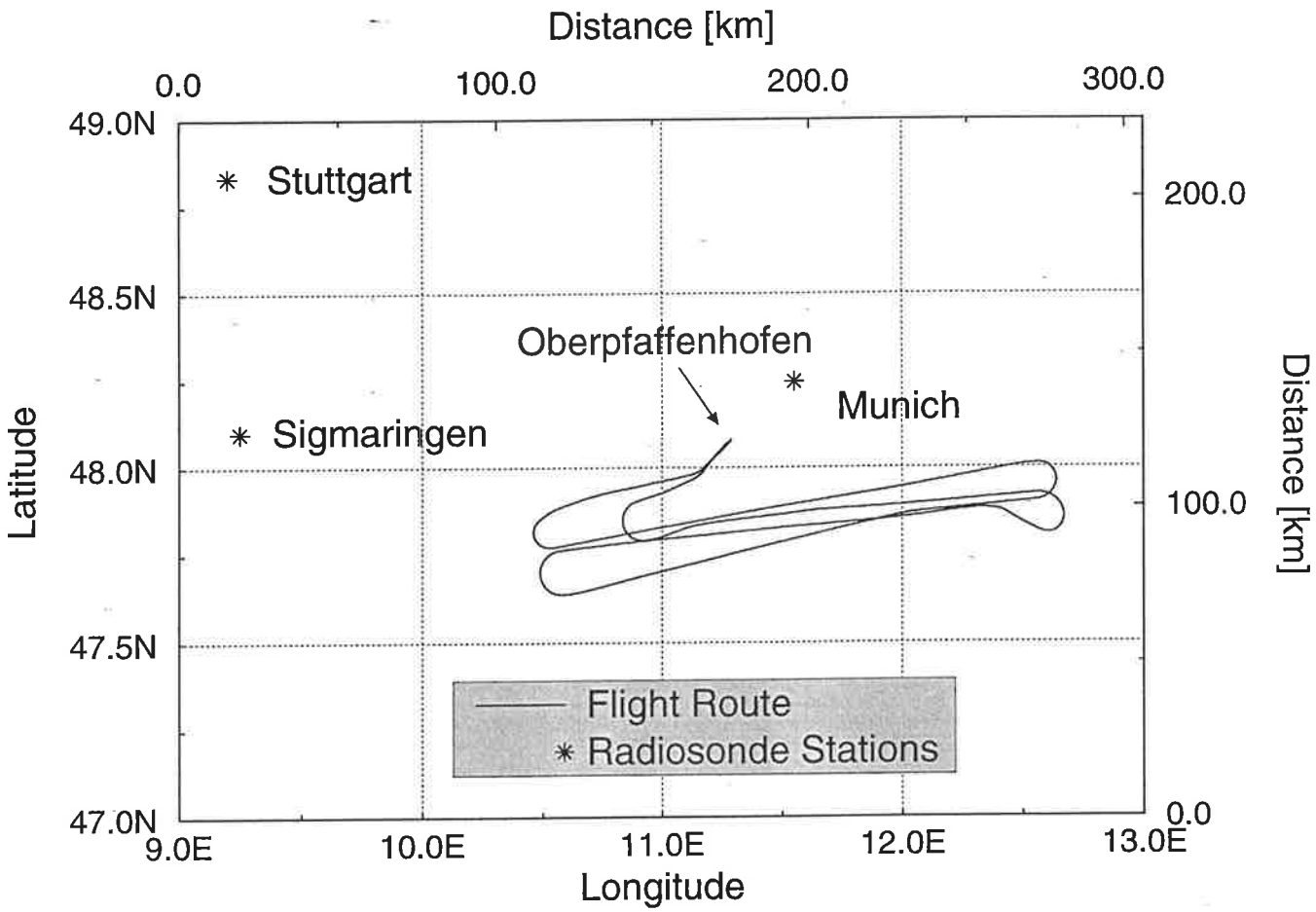
Distance [km]
0.0
100.0
200.0
300.0
49.0N
48.5N
48.0N
47.5N
47.0N
Latitude
Stuttgart
Oberpfaffenhofen
Munich
Sigmaringen
Flight Route
Radiosonde Stations
9.0E
10.0E
11.0E
12.0E
13.0E
Longitude
200.0
100.0
0.0
Distance [km]

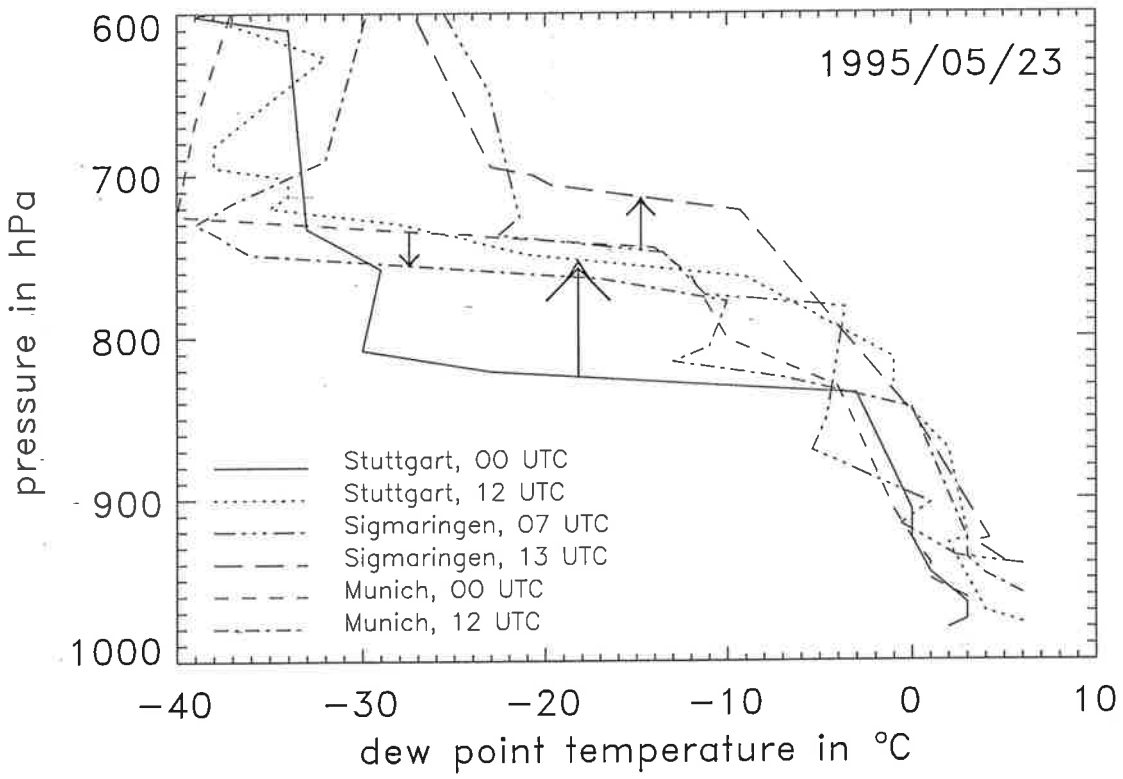
1995/05/23
pressure in hPa
600
700
800
900
1000
−40
−30
−20
−10
0
10
dew point temperature in °C
Stuttgart, 00 UTC
Stuttgart, 12 UTC
Sigmaringen, 07 UTC
Sigmaringen, 13 UTC
Munich, 00 UTC
Munich, 12 UTC

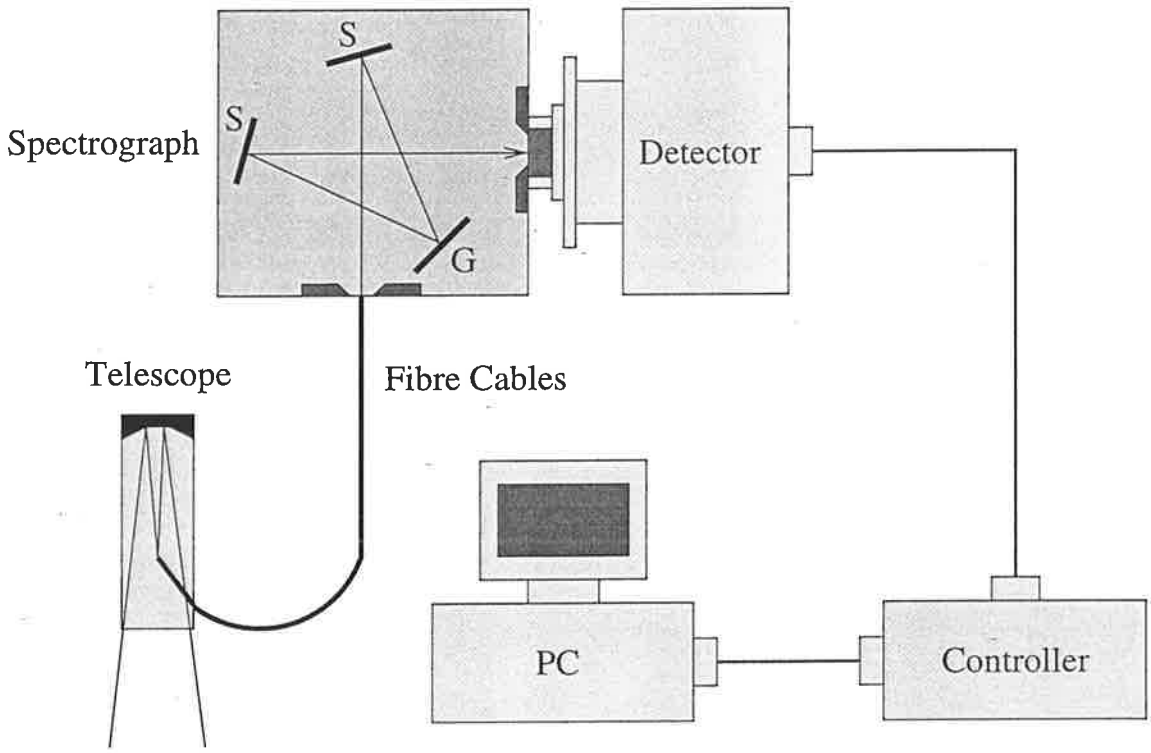
Spectrograph
S
S
G
Detector
Telescope
Fibre Cables
PC
Controller

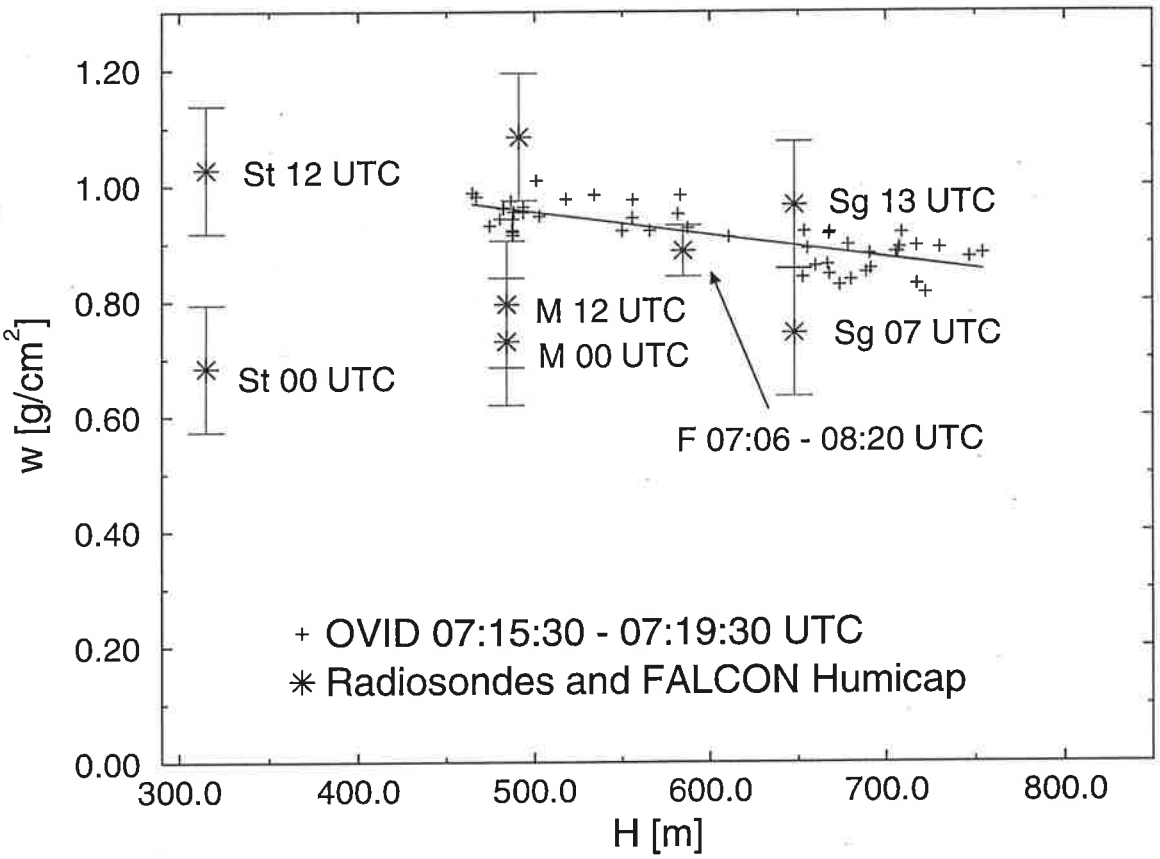
1.20
1.00
0.80
0.60
0.40
0.20
0.00
w [g/cm^2]
300.0
400.0
500.0
600.0
700.0
800.0
H [m]
St 12 UTC
St 00 UTC
M 12 UTC
M 00 UTC
Sg 13 UTC
Sg 07 UTC
F 07:06 - 08:20 UTC
+ OVID 07:15:30 - 07:19:30 UTC
✳ Radiosondes and FALCON Humicap

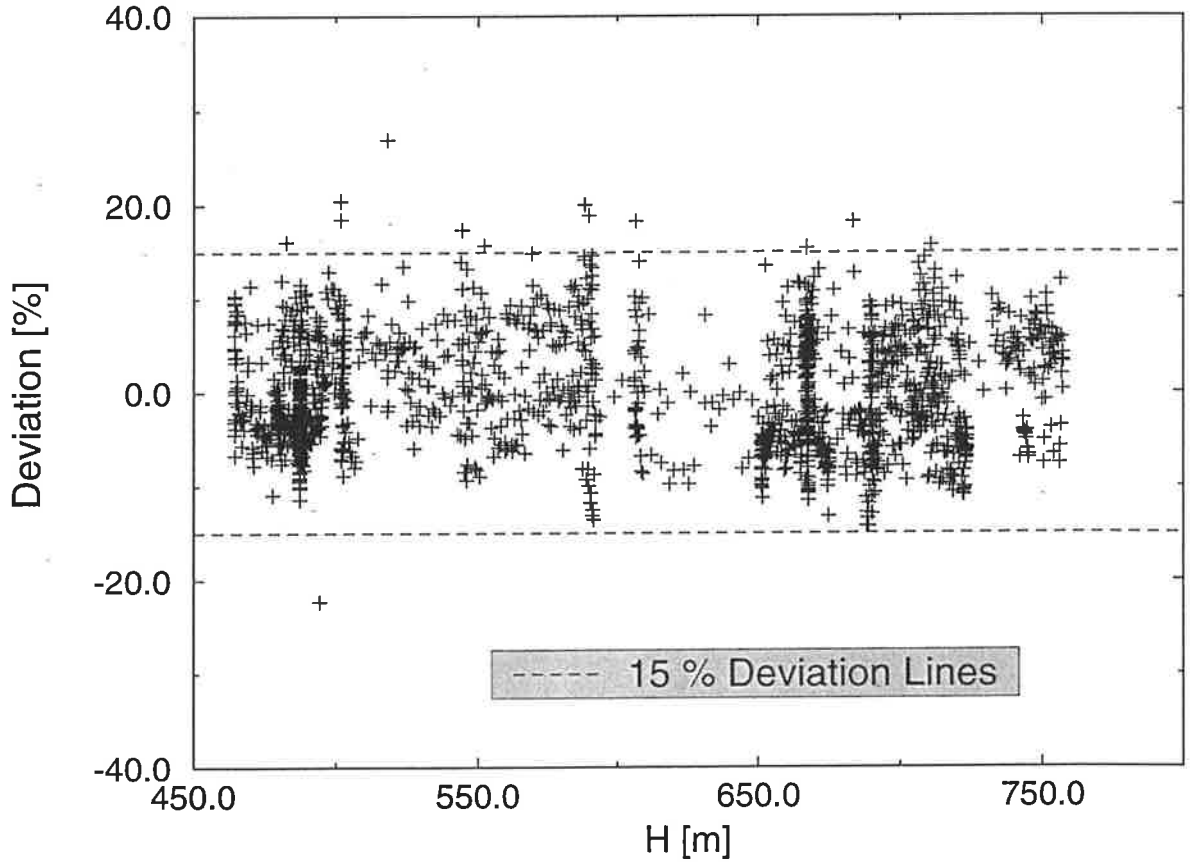
40.0
20.0
0.0
-20.0
-40.0
Deviation [%]
450.0
550.0
650.0
750.0
H [m]
15 % Deviation Lines

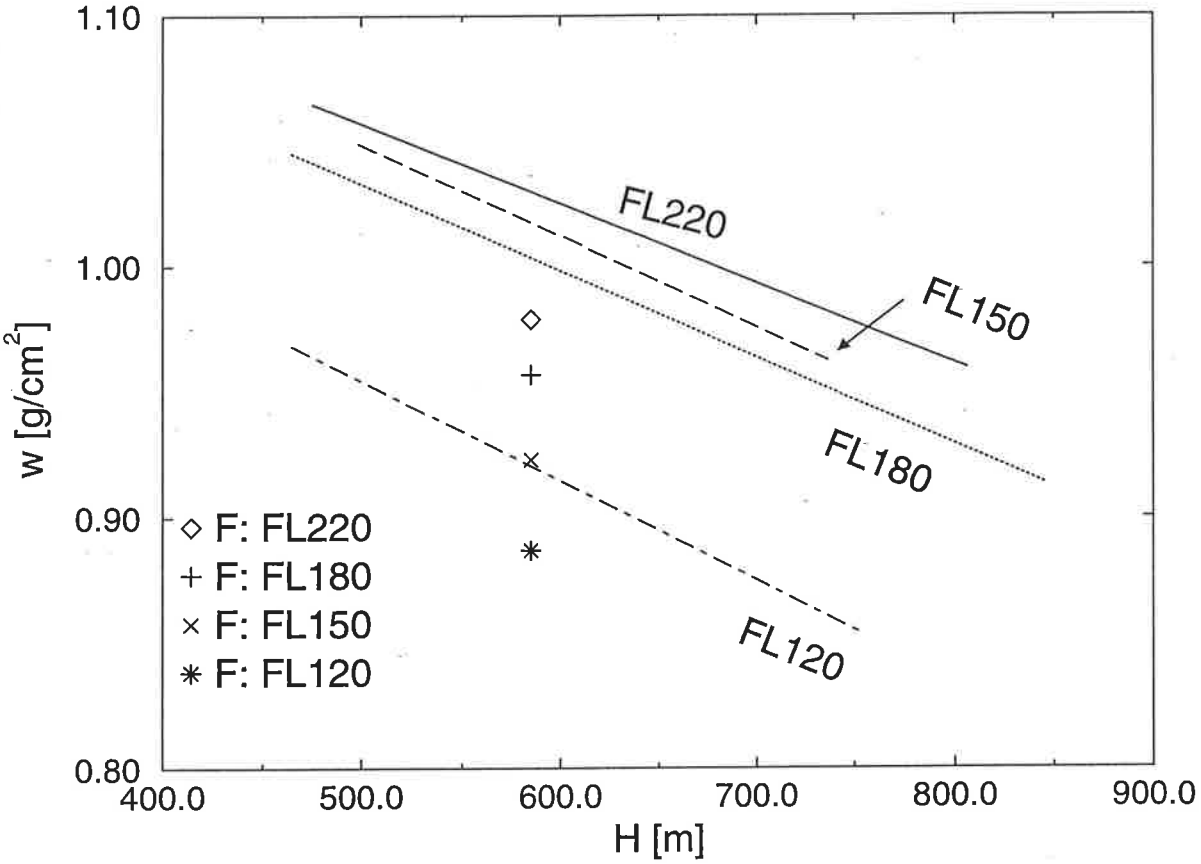
1.10
1.00
0.90
0.80
w [g/cm^2]
400.0
500.0
600.0
700.0
800.0
900.0
H [m]
FL220
FL150
FL180
FL120
◇ F: FL220
+ F: FL180
× F: FL150
∗ F: FL120

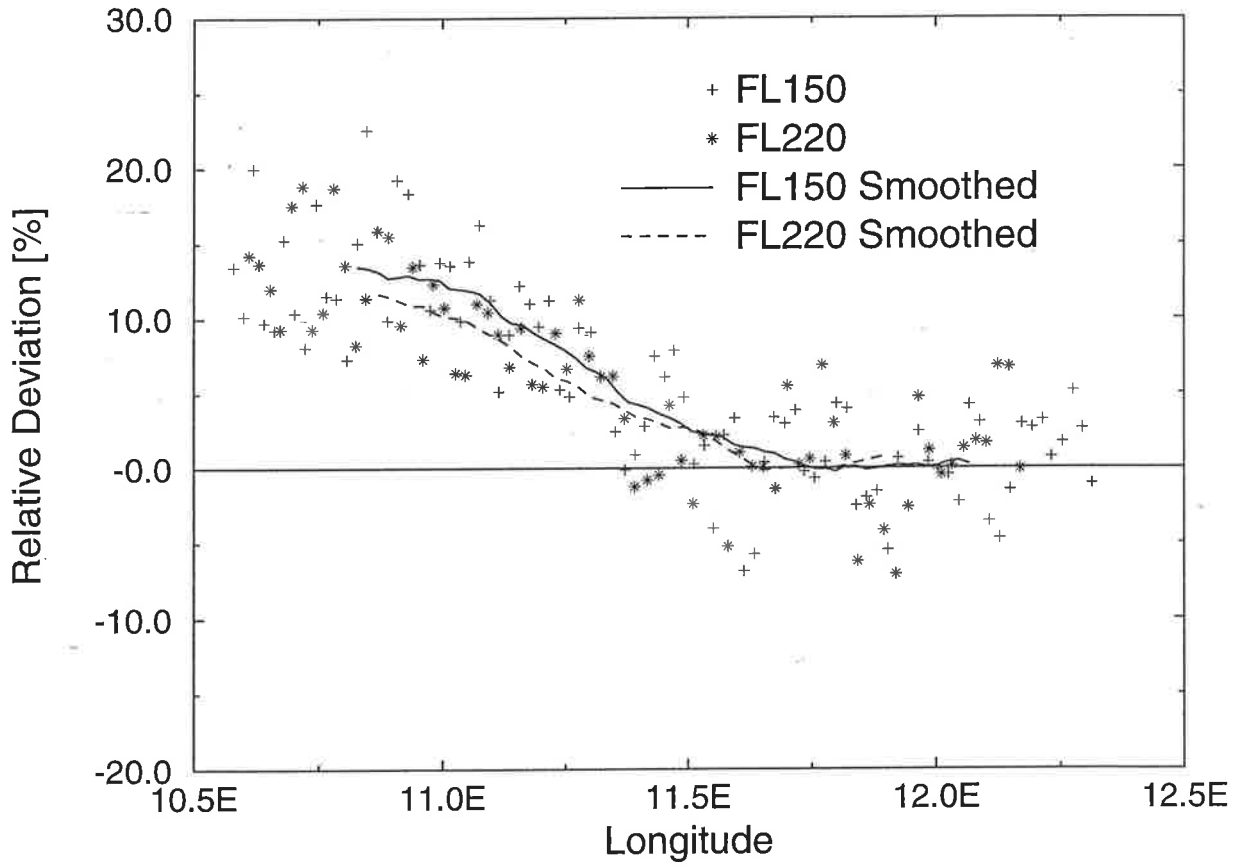
30.0
20.0
10.0
-0.0
-10.0
-20.0
10.5E
11.0E
11.5E
12.0E
12.5E
Longitude
Relative Deviation [%]
FL150
FL220
FL150 Smoothed
FL220 Smoothed

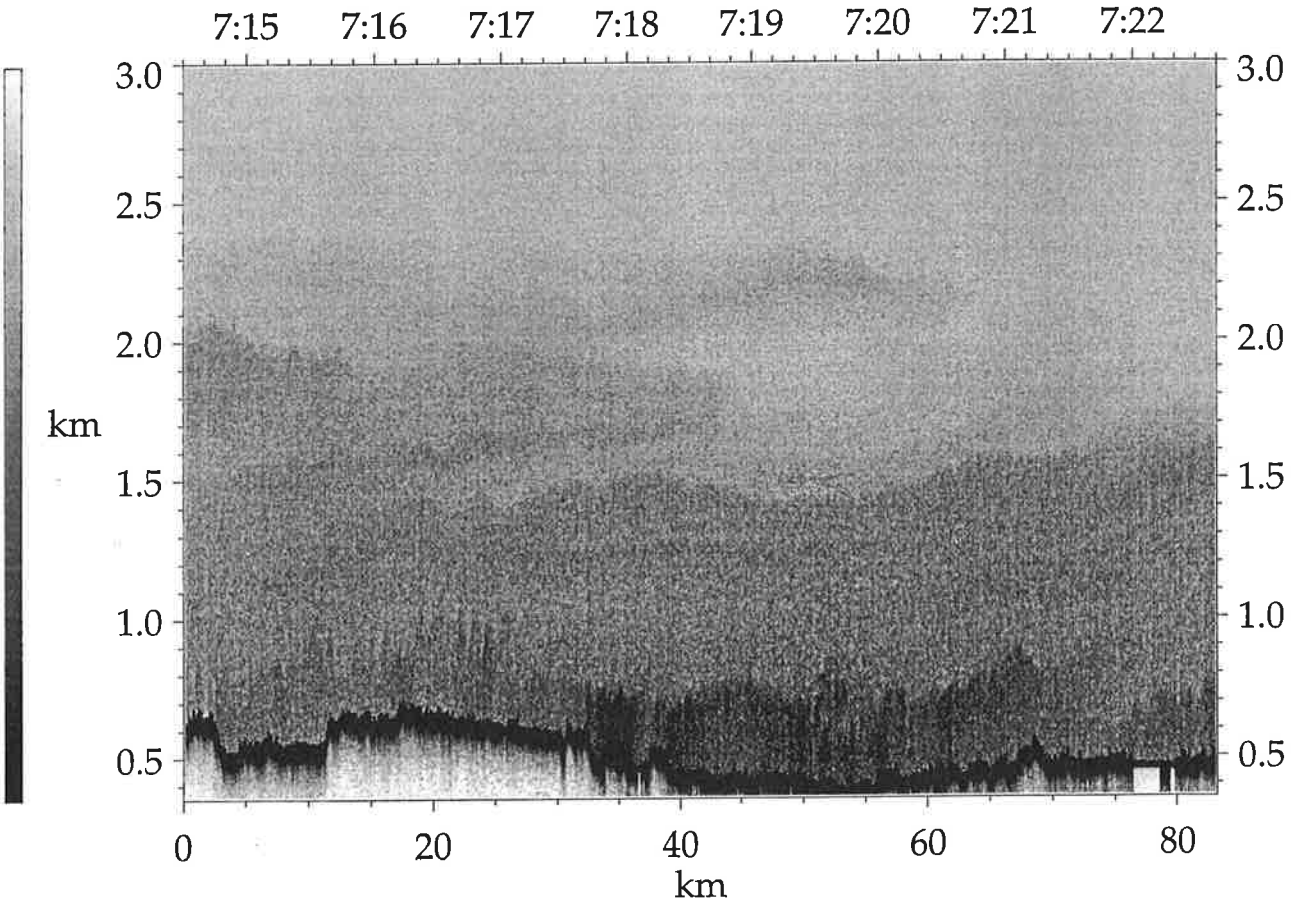
7:15
7:16
7:17
7:18
7:19
7:20
7:21
7:22
3.0
2.5
2.0
1.5
1.0
0.5
km
0
20
40
60
80
km